Journal of Aircraft, Available online 17 July 2025
DOI:10.2514/1.c038402

# Sizing and Mass Estimation of Truss-Braced Wings, Considering Emerging Propulsion Systems

Murat Taflan,*
*Gaziantep University, Gaziantep, 27000, Turkey*
*Cranfield University, Bedfordshire, MK43 0AL, UK*

Howard Smith †
*Cranfield University, Bedfordshire, MK43 0AL, UK*

and
Joseph Loughlan‡
*Loughborough University, Leicestershire, LE11 3TU, UK*

**To advance sustainable and fuel-efficient aircraft, novel configurations such as strut- and truss-braced wings are increasingly being explored. However, conceptual design limitations persist, particularly in the methods for structural sizing and mass estimation of these wings, especially when incorporating emerging propulsion technologies such as electric, hydrogen, and distributed propulsion. This study addresses these gaps by developing a quasi-analytical method for rapid and accurate mass estimation of the wings. Analytical load analysis methods are derived and applied to the structural sizing of struts, juries, and offsets. The proposed method achieves reduced validation errors for wing box, strut, and jury mass compared to existing methods, with an error of -6.77% for total wing mass. With a computation time of just 0.1 seconds per case, it is ideal for early-stage multidisciplinary design optimization. Results indicate minimal weight penalties with distributed propulsion across varying engine counts, along with significant structural efficiency gains for TBW configurations. Underwing fuel tanks on TBW designs further enhance structural and mass efficiency, particularly under dry wing scenarios. Additionally, offset effects reveal a potential reduction in total wing mass while improving aerodynamic efficiency. These findings underscore the promise of TBW designs to support net-zero emissions and drive sustainable aerospace innovation.**

## Abbreviations

| | | |
|---|---|---|
| 2D | = | Two-Dimensional |
| 3D | = | Three-Dimensional |
| ATAG | = | Air Transport Action Group |
| CFD | = | Computational Fluid Dynamics |
| CCW | = | Counterclockwise |
| FEA | = | Finite Element Analysis |
| MDO | = | Multidisciplinary Design Optimization |
| ME | = | Mass Estimation |
| ND | = | Non-dimensional |
| RL | = | Reference Line |
| LE | = | Leading Edge |
| SBW | = | Strut-Braced Wing |
| TBW | = | Truss-Braced Wing |
| TE | = | Trailing Edge |
| WB | = | Wing box |

* Lecturer, Faculty of Aeronautics and Aerospace, Gaziantep University; murattaflan@gantep.edu.tr
† Professor, School of Aerospace Transport and Manufacturing, FRAeS, AIAA Senior Member, Cranfield University.
‡ Emeritus Professor, Department of Aeronautical and Automotive Engineering, FRAeS, CEng, Loughborough University.



Published by AIAA. This is the Author Accepted Manuscript issued with: Creative Commons Attribution License (CC:BY 4.0).
The final published version (version of record) is available online at DOI:10.2514/1.c038402. Please refer to any applicable publisher terms of use.

## I. Introduction

Over the past decades, the cantilever wing and tube configuration has dominated civil aviation. Despite some innovative concepts, their adoption in civilian transport remains limited. The drive to develop more fuel-efficient and environmentally friendly aircraft has persisted, aligning with goals set out by several institutions [1,2], which aim to drastically reduce emissions and noise levels compared to previous years.

To achieve these ambitious targets, research has focused on optimizing traditional aircraft configurations with advanced technologies. However, conventional tube and wing designs may not be sufficient to meet the goals [3,4]. Combining advanced propulsion technologies, such as electric and hydrogen systems [5,6], with novel configurations like the strut-braced wing (SBW) and truss-braced wing (TBW) could offer better fuel efficiency [7] and net-zero emissions. It is essential to consider fuel efficiency since the production of the hydrogen and electric is limited and can release greenhouse gases [6].

Figure 1 illustrates the main components of the cantilever, strut-braced wing (SBW), 1-jury truss-braced wing (1TBW) and 2-jury truss-braced wing (2TBW) configurations following the terminology used in Refs. [8,11]. Both configurations can be designed with or without an offset. These configurations differ from each other with the presence of the juries in TBW as illustrated in Fig. 1.

Previous research indicates that SBW and TBW configurations can significantly enhance fuel efficiency and reduce environmental impact [3,4,8,9]. For instance, NASA's Subsonic Ultra Green Aircraft Research (SUGAR) project found SBW configurations to be the most fuel-efficient among several novel concepts [9]. Similarly, the WeCare project by the German Aerospace Centre (DLR) projected substantial reductions in fuel consumption and NOx emissions with SBW configurations by 2050 [10].

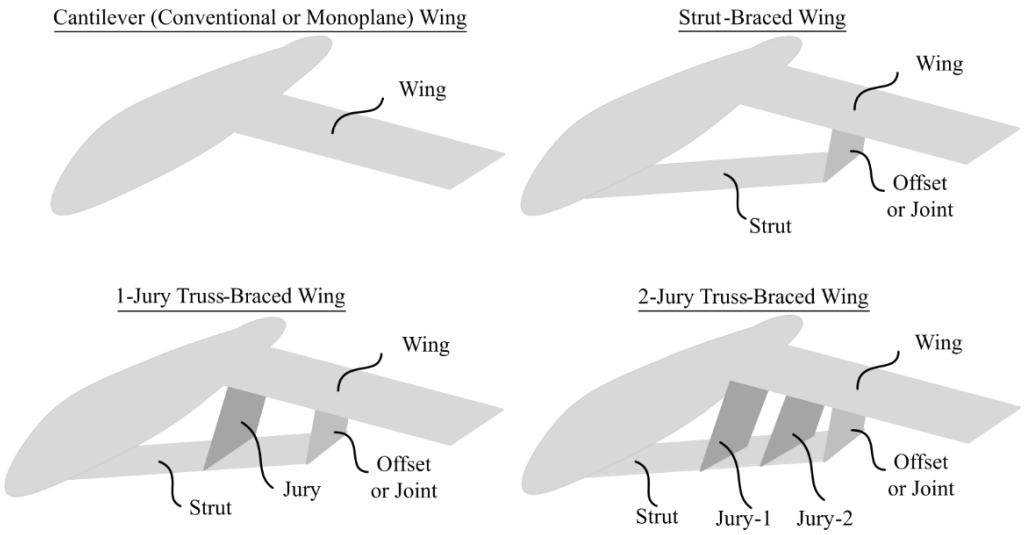


**Fig. 1 Terminology for strut- and truss-braced wing configurations.**

Despite these promising findings, the full potential of SBW and TBW configurations remains underexplored, particularly in integrating advanced propulsion technologies. Emerging hydrogen and electric propulsion technologies have the potential to achieve zero-emissions air transportation and should be considered with novel configurations of SBW and TBW. Electric propulsion technologies facilitate distributed propulsion (DP), which can improve aerodynamic performance [12,13] and reduce fuel consumption. Additionally, hydrogen propulsion systems necessitate cryogenic tanks, making traditional wing storage infeasible and leading to the concept of dry wings. Both distributed propulsion and dry wings must be explored in design studies to understand their impact on the performance of the aircraft with SBW or TBW.

Accurate design and performance analysis of SBW and TBW requires advanced conceptual or preliminary methods to balance lift-induced drag, interference drag, and structural mass [14,15]. However, existing structural sizing and mass estimation methods for SBW and TBW, especially with electric, hydrogen, or distributed propulsion systems, have significant limitations.

This study reviews existing mass estimation methods for SBW and TBW, identifies their limitations, and introduces a quasi-analytical mass estimation method tailored for these configurations with advanced propulsion technologies. The proposed method provides detailed structural sizing and mass estimations for strut, jury, and offset components, demonstrating computational efficiency and accuracy suitable for multidisciplinary design optimization (MDO) studies. The study also examines the effects of distributed propulsion and dry wing concepts on the masses of cantilever and TBW configurations, applying the proposed methods to these scenarios.

### A. Previous Studies on Mass Estimation

Previous studies have been reviewed, and the limitations and gaps were identified. Mass estimation methods for SBW and TBW are grouped into empirical-based, analytical-based, and finite element analysis (FEA)-based methods following Ref. [16]. Limitations in analytical load analysis and structural sizing methods are also indicated.

*1. Empirical and Semi-Empirical Methods*

Empirical methods typically use regression analysis on historical data, while semi-empirical methods combine empirical data with physics-based governing equations. These methods are suitable for initial design stages but lack the accuracy needed for novel configurations due to insufficient historical data. Previously, Smith et al. developed an empirical method for SBW [17], but further validation is needed [18]. Chiozzotto developed a semi-empirical method [19],based on data generated using physics-based methods [18,20]. Error margin of the method in estimating the total masses of the strut and jury requires the development of more detailed methods with higher accuracy.

*2. Analytical and Quasi-Analytical Methods*

Analytical methods involve detailed structural sizing under various loading conditions, and quasi-analytical methods blend analytical and empirical approaches to enhance accuracy and computational efficiency. Early studies by Jobe *et al.* [21] and Naghshineh-Pour [22] demonstrated the benefits of strut implementation in reducing material mass [21–23], highlighting the need for detailed structural analyses [21]. Locatelli *et al*. [24] improved accuracy with a rectangular box model but required further validation. Mallik *et al.* [25] enhanced rectangular box model by incorporating buckling considerations in the skin panel sizing. Chiozzotto [18,20] contributed to the structural design and mass estimation of SBW and TBW by incorporating static aeroelastic effects into the ME method. Despite achieving reasonable accuracy, the method exhibited an average error of 10.6% in total wing group masses, indicating the possible refinements, particularly in the sizing of truss components such as the strut and jury.

*3. FEA Based Methods*

FEA-based methods offer high accuracy but are computationally intensive. Bhatia *et al.* [26] included flutter and buckling constraints in an MDO tool but faced issues with convergence and computational time. Zhang *et al.* [27] used topology optimization in ANSYS but neglected torsional effects. Dorbath [28] employed a high-fidelity physics-based approach, validated using real aircraft data. While highly accurate, the method required considerable computational effort, with a runtime of 24 hours. Similarly, computational times spanning several hours were reported by Hürlimann *et al.* [29], and durations extending to days were noted by Benaouali and Kachel [30]. These findings underscore the trade-off between achieving high accuracy and maintaining computational efficiency.

*4. Strut Reaction Force*

The strut reaction force should be known to determine both the load relief provided to the wing and the loads carried by the strut itself. The computation of the strut reaction force is one of the challenges in analytical structural sizing and mass estimation methods. The fixed attachment of the wing to the fuselage in an SBW configuration causes a statically indeterminate structural problem increasing the complexity of calculating the strut reaction force which is required in the conceptual or preliminary sizing stages. In the literature, the strut reaction force has been defined as a user input [22], using an iterative approach [24] or calculated by applying beam equations [31] on simplified SBW models with one concentrated load on a half wing. Castigliano's second theorem has also been used in previous studies [32]. The analytical approaches of beam equations or Castigliano's approach have advantages over FEA approaches due to their fast computation time and reduced complexity in implementation. A limitation is observed in analytical strut reaction force calculation in an SBW or TBW with more than one concentrated load.

*5. Offset*

Studies have shown that the interference drag at the strut-wing joint significantly impacts aerodynamic performance. Tetrault *et al.* [33] and the following research highlighted the importance of the strut angle and cross-section in reducing drag [4,34–36]. Incorporating an offset, as illustrated in Fig. 1, also minimize interference drag and improve aerodynamic efficiency and the effect of offset on the wing mass should be studied subsequently [37]. However, the literature review revealed the gaps in structural sizing and mass estimation methods for an offset.

**B. Introduction to the Advanced Quasi-Analytical Method**

Based on the outcomes of previous mass estimation research for SBW and TBW, the need arises for analytical or quasi-analytical methods considering the computational time and accuracy. These methods offer a better balance between accuracy and complexity, positioned between simpler empirical methods and more intricate finite-element-based methods [38,39]. Such methods could be developed to be responsive to specific aircraft design parameters and emerging technologies while surpassing the accuracy of both empirical and FEA-based methods [40]. They can utilize the analytical structural sizing approaches to estimate the mass of primary structures such as load-carrying boxes of wing, strut, offset, and jury, while the empirical or semi-empirical methods are used for the mass estimation of secondary structures. The requirements of the proposed advanced method are listed as follows.

*Emerging Propulsion Technologies:* The literature review revealed the gaps in the mass estimation of SBW and TBW with electric, hydrogen and distributed propulsion systems. Hence, the proposed method should be sensitive to the effects of emerging propulsion technologies and dry wings.

*Computational Efficiency, Accuracy and MDO Studies:* The long computational times of FEA-based methods have been noted in the literature review. Thus, the proposed method should be computationally efficient and accurate enough to be used in conceptual or preliminary MDO studies while having minimal complexity in implementation.

*Complete Component Coverage:* The proposed method should provide accurate enough and detailed structural sizing and mass estimation for all primary structural components of struts, jury, offset, and wing. Detailed structural sizing enables accurate mass estimation and a more precise assessment of their impact on aircraft performance and broadens the space for design exploration studies.

*Analytical Solutions for Critical Components:* In addition to the classical load analysis procedures of a cantilever wing aircraft, the SBWs and TBWs require additional load analysis due to the presence of the strut, jury and offset. The method should include an analytical solution for the strut reaction force on SBW and TBW accommodating an unlimited number of concentrated loads of engines, underwing fuel tank (drop tanks) or other external loads. This is essential for accurately modelling the impacts of distributed propulsion systems on the structural mass of SBW and TBW. Similarly, analytical solutions are also required in the load analysis of the juries and offsets.

*Validation and Application:* Detailed validation, verification and application of the proposed method are required to evaluate accuracy, computational speed, practical usability, and credibility.

These requirements can be achieved by modifying and upgrading an existing quasi-analytical mass estimation method initially developed for cantilever wings. For such an upgrade and improvement of existing methods, this study presents the development and application of quasi-analytical mass estimation methods for the struts, juries, and offsets of a TBW considering the integration of electric, hydrogen, and distributed propulsion systems. To achieve the complete mass estimation of a TBW, the developed methods will then be integrated with existing mass estimation techniques for cantilever wings to enhance their coverage for SBW and TBW. The selected existing ME method is called the "baseline method" in this study and is explained briefly in the following section.

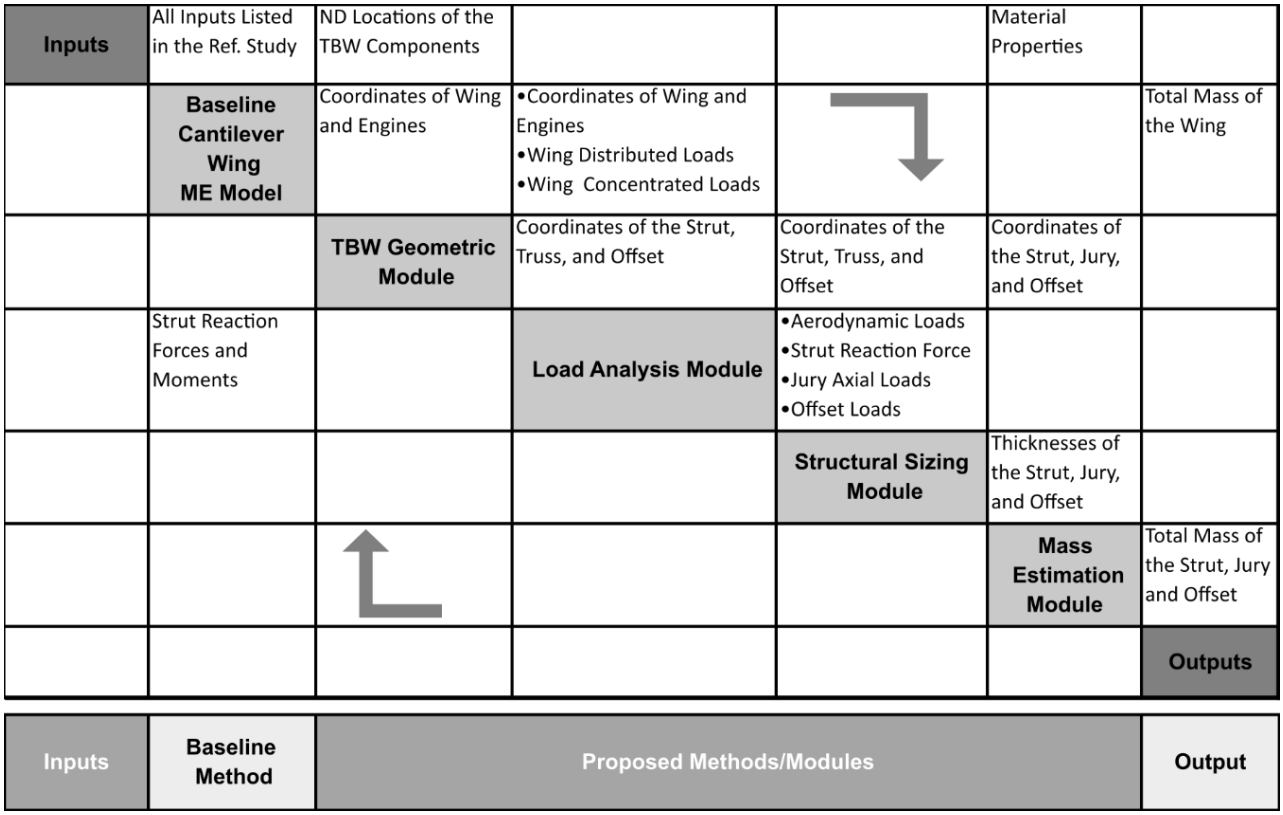


**Fig. 2 N2 diagram of the TBW mass estimation methods and their integration with the baseline method.**

## C. Baseline Method

Considering the above-listed requirements, the ME method for cantilever wings from Ref. [41] is selected as the baseline method. The baseline method was developed considering its future applications for SBW and TBW with electric, hydrogen, and distributed propulsion systems. It consists of modules for geometric modelling, load calculation, structural sizing, and mass estimation. This method presented high accuracy with an average error of -2.2% and a standard error of 1.8% in estimating the wing group masses of thirteen

different aircraft with cantilever wings from different categories. The method's high sensitivity to the design parameters of an aircraft with conventional and strut-braced wings was also presented in Ref. [42]. However, the proposed method lacks the mass estimation of the strut, jury offset, and the strut- or truss-braced wings with distributed propulsion systems. Hence, it will be modified and improved with the methods presented in this study.

### D. Development and Implementation

This section briefly introduces the methods developed in this study, their application as software and integration with the baseline method. The proposed method consists of four main modules as depicted with a N2 chart in Fig. 2.

*The TBW Geometric Module* utilizes the geometric models developed in Section II for the strut, jury, and offset. It receives the coordinates of the wing and engines from the baseline method and computes the coordinates of the strut, jury, and offset including the dimensions and locations of their primary structures.

*The Load Analysis Module* uses the coordinates and dimensions of the components from the geometric module and the concentrated and distributed loads for a specific flight case to compute the strut reaction force and other loads acting on the strut, jury, and offset with the methods explained in Section III. The strut reaction force is also transferred to the baseline method, to be used in the shear force, and moment calculations of the wing.

*The Structural Sizing Module* uses the dimension and load data from the Load Analysis Module and sizes the thicknesses of the primary structures considering the constraints explained in detail in Section IV .

*The Mass Estimation Module* receives the calculated dimensions of the primary structures from the Structural Sizing Module and computes their masses using the material density and volume. It then computes the secondary structures' masses with semi-empirical methods to compute the total masses of strut, jury, and offset. These methods are explained in Section V.C. The total group masses of the SBW or TBW are then computed by summing the computed mass values of the strut, jury, and offset and the mass of the wing value transferred from the baseline method.

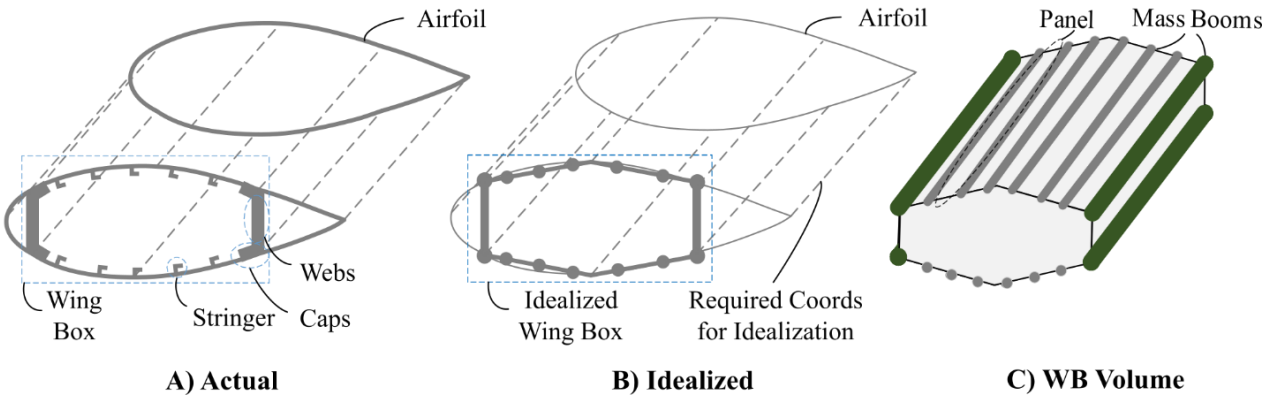


**Fig. 3 Illustration of the wing box idealization and the comparison between the actual and idealized wing box sections [41].**

## II. Geometric Models

Three-dimensional (3D) geometric models are developed and introduced in this section for strut, jury, and offset. The load carrying box of the strut, jury, and offset are modelled as rectangular box while the hexagonal wing box (WB) model of the baseline method [41] shown in Fig. 3 is used for the wing.

### A. Rectangular Box Model

Considering the trade-off between the computational time and the model accuracy, a uniform, and one-section geometric model is generated for the strut, jury and offset with rectangular load carrying boxes (shown in Fig. 4) different from the discretized wing model of the baseline method with a hexagonal WB model shown in Fig. 3. The rectangular box model reduces complexity in implementation and computational time. The non-dimensional (ND) locations of the forward ($\xi_{Comp,fs}$) and the rear spars ($\xi_{Comp,rs}$) as a fraction of the chord of the component are variable. $t_{Comp,Skin}, t_{Comp,Box}, w_{Comp,Box}$ are the skin thickness, thickness, and width of the rectangular box, respectively.

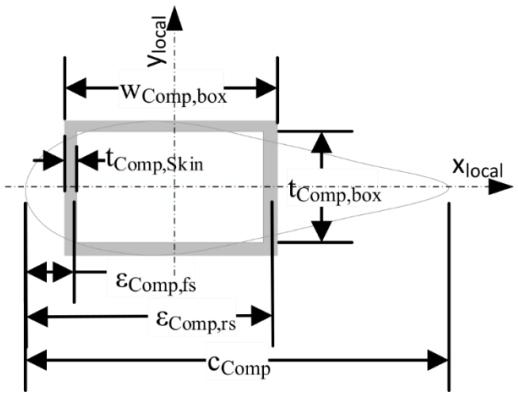


**Fig. 4 Strut and offset structural box model.**

## B. Strut Geometric Model

The two-dimensional (2D) top and front views of the strut geometric model and its attachment to the wing with an offset are illustrated in Fig. 5. Without an offset, the strut is directly connected to the wing. The offset changes the coordinates of the strut tip in the x and z axes and the root in x axis, depending on the offset height and sweep angle.

The input parameters for the strut are ND strut position along the wing as a fraction of half wing span length, $\Lambda_{Strut}$, ND chordwise position of the strut as a fraction of the local wing section chord, $\varepsilon_{Strut}$, strut chord ratio to the wing local chord where the strut is attached, $\tau_{StrutWing}$, strut thickness to chord ratio,$\tau_{Strut}$, strut sweep angle (from the top view, counterclockwise (CCW) direction is positive), $\Theta_{Strut}$, the distance of the strut root to the aircraft centre line in the y-axis, $y_{Strut,Root}$ and in z-axis, $z_{Strut,Root}$.

The coordinates of the strut root are defined with its design variables of $y_{Strut,Root}$ , and $z_{Strut,Root}$. Then $x_{Strut,Root}$ can be calculated considering the trigonometric relations with $y_{Strut,Root}$ , $z_{Strut,Root}$, the strut sweep angle ($\Theta_{Strut}$, ) and the offset coordinates considering the presence of the offset. When the coordinates of the root and tip of the strut are calculated, the strut reference line (RL) can be generated at the centre of the strut box. Hence, using the chord, thickness and spar positions of the strut, its 3D view can be generated including root chord, tip chord, spars, leading edge (LE), and trailing edge (TE).

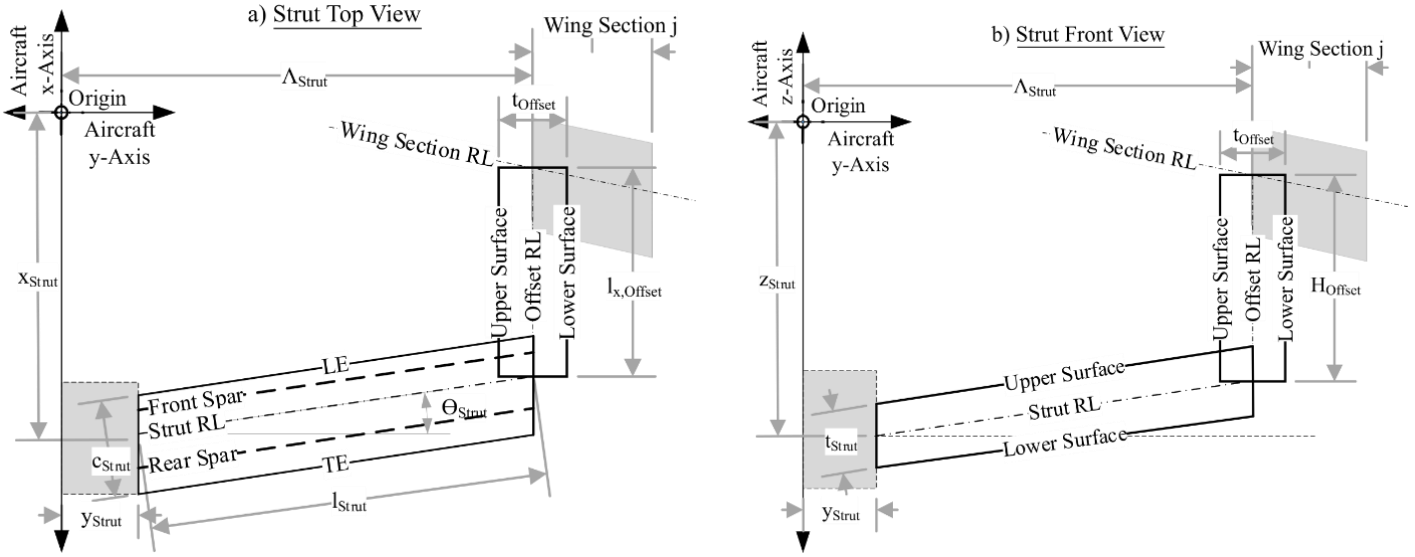


**Fig. 5 2D views of the SBW geometric model: a) top view and b) front view.**

## C. Offset Geometric Model

The offset geometric model is shown in Fig. 6, where $H_{Offset}$ is the offset height in the global z-axis direction and $\Theta_{Offset}$ is offset angle around the global y-axis (from the side-view, CCW is positive), and $l_{Offset}$ is the length of the offset. Other design variables are the offset thickness to chord ratio $(\tau_{Offset})$, and offset chord ratio to the wing local chord where the offset is attached ($\tau_{OffsetWing}$).

The root of the offset is where it is connected to the strut, and it can be found with simple trigonometric relations using $H_{Offset}$ and $\Theta_{Offset}$. The coordinates of the tip of the offset can be computed using $\Lambda_{Strut}$ and $\varepsilon_{Strut}$. If the wing is designed with the offset, the

coordinates of the strut tip will be equal to the computed coordinates of the root of the offset. After computing the offset's tip and root coordinate points, an offset reference line passing through these points can be generated. Then the spars of the offset can be located as a fraction of the offset chord from the LE edge of the offset.

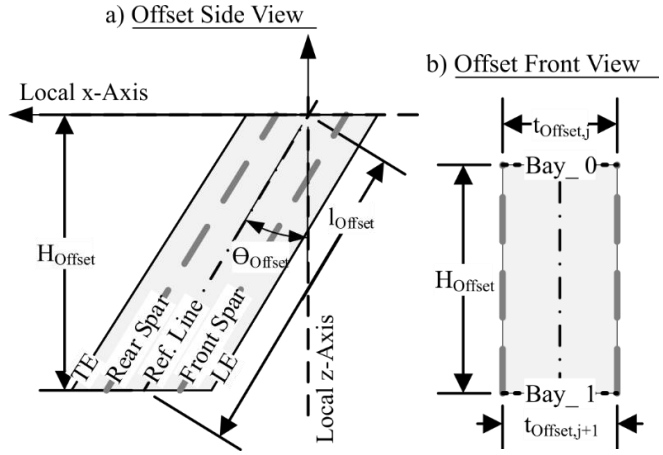


**Fig. 6 Views of the offset geometric model: a) side view and b) front view.**

## D. Jury Geometric Model

The juries are located between the reference lines of the strut and wing. They can be designed either perpendicular to the wing reference line (jury-1) or perpendicular to the strut reference line (jury-2), as shown in Fig. 7. Each jury has four design variables of jury direction (either perpendicular to the strut or the wing), jury chord ratio to that of the strut $\tau_{JuryStrut}$, jury thickness to chord ratio $\tau_{Jury,j}/c_{Jury,j}$, and ND jury root position ($\Lambda_{Jury,Root,i}$) in the y-axis as a fraction of the distance ($\Delta y_{Strut}$) between coordinates of the strut tip ($y_{Strut,Tip}$) and the root ($y_{Strut,Root}$) on the global y-axis. After computing the tip and root coordinate points of the juries, a jury reference line can be generated between these two points. Then the spars of the jury can be located as a fraction of the jury chord from the LE edge of the jury.

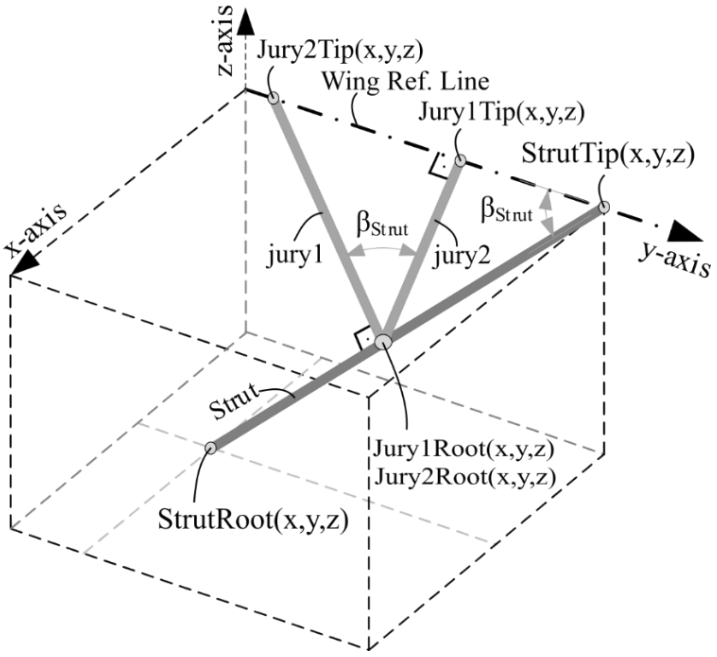


**Fig. 7 Directions and coordinates of the juries: (jury-2) perpendicular to the wing reference line and (jury-1) perpendicular to the strut reference line.**

## III. Load Analysis

Strut, jury and offset need to resist the external aerodynamic loads and the internal structural reaction forces. The types of loads acting on each truss component, as considered in this study, are listed in Table 1. The computation methods of those loads are explained in this section.

**Table 1 The list of the loads acting on the truss components.**

| Components | Loads |
|---|---|
| Strut | Reaction force caused by the wing and fuselage<br>Aerodynamic loads |
| Jury | Reaction force caused by the strut and wing<br>Aerodynamic loads |
| Offset | Reaction force caused by the wing and strut<br>The bending moment caused by the strut reaction<br>Aerodynamic loads |

### A. Aerodynamic Loads on Truss Components

Although the truss components (jury, offset and strut) of a TBW are structural elements and generally not designed to generate lift, they are still prone to aerodynamic loads in different flight cases. These aerodynamic loads are considered in their structural sizing using a conservative, simplified approach. The lift generated by these components ($L_{Comp.}$) is computed with $L_{Comp.} = C_{L,max,Comp} q_\infty S_{Comp}$, where $C_{L,max,Comp}$ is the maximum lift coefficient of the component, $q_\infty$ is dynamic pressure of the flight case and $S_{Comp}$ is the area of the lifting surface. For a conservative load analysis approach, the lift distribution can be assumed as triangular with zero load intensity at the supports and a maximum value at the midpoint. For this load distribution the highest bending moment ($M_{Comp}$) can be computed with $M_{Comp} = L_{Comp} l_{Comp}/6$ at the middle of the component where $l_{Comp}$ is the length of the component.

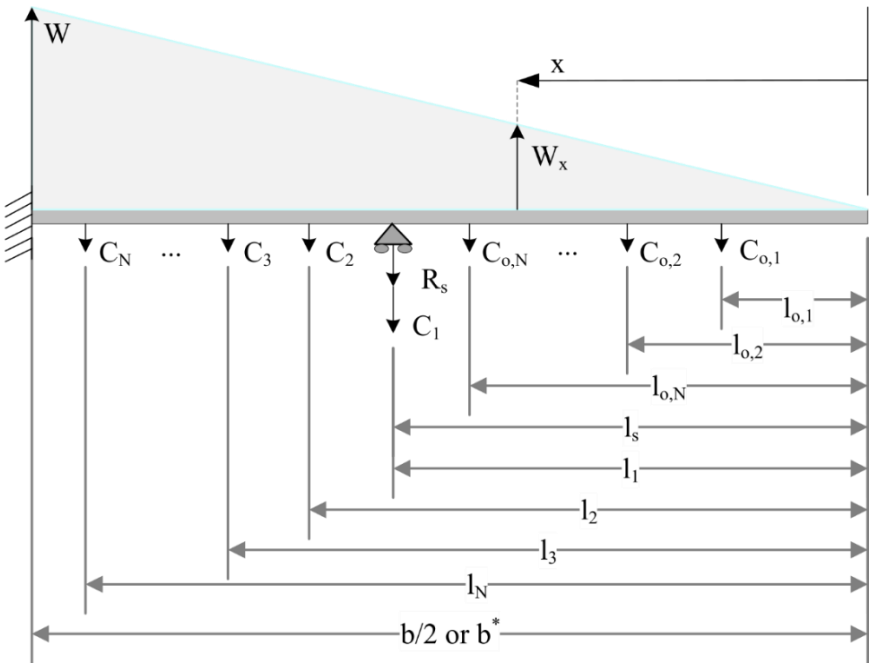


**Fig. 8 Illustration of the simplified TBW model with an unlimited number of concentrated loads.**

### B. Strut Reaction Force

The analytical solutions discussed in Section I.A.4 typically address models with a single concentrated load [18,31,32]. When the number of concentrated loads increases or their positions change, these methods become invalid. Therefore, in this study, a more general analytical solution is developed using Castigliano's second theorem [43] to compute the strut reaction force in an SBW model with any

number of concentrated loads (Fig. 8), which is essential for studying the effects of distributed propulsion systems. The analytical solutions will be validated against FEA results. In the application of Castigliano's theorem to the TBW configuration, the following assumptions are made for simplification.

- The model includes both distributed and concentrated loads placed at the WB reference line.
- The total distributed load along the wing under a specific load case provided from the baseline method is redistributed in a triangular shape with the same total magnitude as shown in Fig. 8 to simplify the analytical derivations.
- The beam is assumed uniform between the wing root and the strut-wing attachment point.
- The effects of juries on the strut reaction force calculation are neglected for the TBW models.

Castigliano's second theorem states that the partial derivative of the total strain energy for the applied load is equal to the displacement at the point of load application. This leads to the equation Eq. (1) which computes the deflection at the strut-wing attachment point, $\Delta_s$. In addition to the above-discussed simplifications, if the deflection of the wing at the strut attachment point, $\Delta_s$, is assumed to be zero, Eq. (1) can be rearranged as Eq. (3) to compute the strut reaction force $R_s$ in the simplified indeterminate SBW problem illustrated in Fig. 8. The negligible effect of the zero deflection assumption on the computed strut reaction force in a SBW is previously validated in Ref. [31]. This assumption simplifies the solution of statically indeterminate SBW configuration with any number of concentrated loads under various flight cases discussed in Section IV.A while preserving essential structural behaviour.

$$\Delta_s = \int_0^{b^*} M\left(\frac{\partial M}{\partial R_s}\right)\frac{dx}{EI} \tag{1}$$

In Eq. (1), $M$ is the moment along the wing model in Fig. 8, $R_s$ is the strut reaction force, $E$ is the modulus of elasticity, and $I$ is the moment of inertia. Equation (1) can be rearranged as Eq. (2) for the unlimited number of concentrated loads located at the inner and outer parts of the wing using the boundary conditions shown in Fig. 8. The inner part is between the strut-wing attachment point and the aircraft centreline and the outer part is from the strut-wing attachment point to the wing tip as shown in Fig. 8.

$$\Delta_s = \int_0^{l_{0,1}} M_{0,1}\left(\frac{\partial M_{0,1}}{\partial R_s}\right)\frac{dx}{EI} \ldots + \int_{l_{0,N}}^{l_s} M_{0,N}\left(\frac{\partial M_{0,N}}{\partial R_s}\right)\frac{dx}{EI} + \int_{l_s}^{l_2} M_1\left(\frac{\partial M_1}{\partial R_s}\right)\frac{dx}{EI} \ldots + \int_{l_N}^{b^*} M_N\left(\frac{\partial M_N}{\partial R_s}\right)\frac{dx}{EI} \tag{2}$$

where $M_{0,1}, \ldots, M_{0,N}$ are the moment equations between the concentrated loads of $C_{0,1}$ and $C_{0,N}$ at the outer wing section and $M_1, \ldots, M_N$ are the moment equations between the concentrated loads of $C_1$ and $C_N$ at the inner section. The distances from the wing tip to the concentrated loads located at the outer and inner wing sections are denoted by $l_{o,1}, \ldots l_{o,N}$ and $l_1, \ldots l_N$, respectively, as shown in Fig. 8. The distance from the strut attachment point to the wing tip is denoted by $l_s$. The distance of the concentrated load located at the strut attachment point is also denoted by $l_1$.

After deriving the moment equations along the wing and substituting in Eq. (2), Eq. (3) is derived for analytical computation of the strut reaction force ($R_s$) in the simplified indeterminate SBW structural model with multiple concentrated loads illustrated in Fig. 8.

The analytical solution in Eq. (3) is validated by comparing its result to the strut reaction force value obtained from an FEA analysis using the beam model shown in Fig. 8. Table 2 presents the input parameters, their description and values used in the validation study. The validation results are shown in Table 3 with a difference of -0.41% between the results of the FEA and analytical solutions.

$$\begin{aligned} R_s = \Bigg[ & -\frac{{l_s}^5 W}{120 b^*} + \frac{l_s {b^*}^3 W}{24} - \frac{{b^*}^4 W}{30} + \sum_{k=1}^{N_o} C_{o,k}\left(\frac{{l_s}^3}{6} - \frac{l_s {b^*}^2}{2} + \frac{{b^*}^3}{3}\right) + \sum_{k=1}^{N_o} C_{o,k} l_{o,k}\left(-\frac{{l_s}^2}{2} + l_s b^* - \frac{{b^*}^2}{2}\right) \\ & + l_s \sum_{k=1}^{N_{in}}\left(-\frac{{l_k}^2}{2} C_k\right) - \sum_{k=1}^{N_{in}}\left(-\frac{{l_k}^3}{6} C_k\right) + \sum_{k=1}^{N_{in}} C_k\left(-\frac{l_s {b^*}^2}{2} + \frac{{b^*}^3}{3}\right) \\ & + \sum_{k=1}^{N_{in}} C_k l_k\left(l_s b^* - \frac{{b^*}^2}{2}\right)\Bigg] \Big/ \left[\frac{{l_s}^3}{3} + l_s {b^*}^2 - {l_s}^2 b^* - \frac{{b^*}^3}{3}\right] \end{aligned} \tag{3}$$

The reaction forces of the strut ($R_S$) are calculated in the global z-axis, which should be transformed to the local axis of the strut (reference line) using well known 3D rotation matrix. In the presence of the offset, the reaction force should, similarly, be transformed to the local reference axis of the offset. In this case, the resultant force on the strut should be computed. The resultant force is used to compute the bending moment and torsion acting along the offset and the bending moment transferred to the wing.

**Table 2 Input parameters (shown in Fig. 8) used for the validation of the simplified models.**

| Description | Inputs | Value |
|---|---|---|
| The distance of the strut to the wing tip | $l_s$, mm | 25,000.0 |
| The distance of the concentrated load to the wing tip | $l_2$, mm | 42,500.0 |
| The half span length of the wing | $b^*$, mm | 50,000.0 |
| The weight of the concentrated load located at the inner wing section | $C_2$, N | 1,000.0 |
| The magnitude of the distributed load at the root | $W$, N/mm | 0.04 |

**Table 3 Comparison of the strut reaction forces obtained from the analytical models and FEA.**

| | Strut reaction force, N | Difference |
|---|---|---|
| Analytical solution | 491.00 | |
| FEA | 489.00 | -0.41% |

### C. Axial Loads on Juries

The juries are supportive structural components in a TBW configuration increasing the critical buckling load of the strut by reacting to the forces emerged from the buckling of the strut. This section explains the development of a conservative analytical solution to compute axial reaction forces acting on a jury. As previously explained, the juries can be positioned either perpendicular to the wing or perpendicular to the strut. The effects of both orientations are considered in the derived analytical solutions.

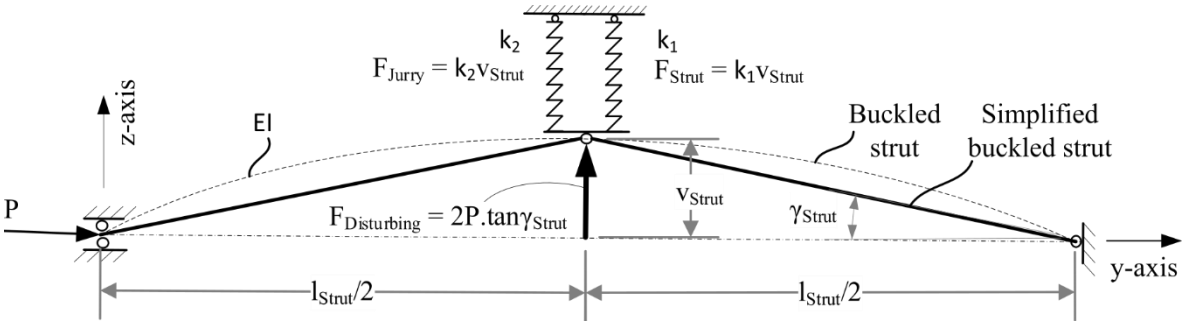


**Fig. 9 First buckling mode of the strut column in the simplified TBW model with one jury support.**

*1. One Jury Model*

The buckling mechanism of the strut can be simplified as shown in Fig. 9, where the bending stiffness of the strut is represented by the spring with a stiffness of $k_1$. The force generated by the spring is $F_{Strut} = k_1 v_{Strut}$ and it resists the disturbing load, $F_{Disturbing}$, caused by the axial compressive loads $P$ applied to the strut. If $F_{Strut}$ is equal to $F_{Disturbing}$, the condition is called neutral equilibrium, and the load $P$ is equal to $P_{cr}$ which is also called as bifurcation point [44]. Any increase in $P$ after the bifurcation point will make the system unstable, and a sudden buckling will occur.

If a jury with an axial stiffness of $k_2$ is added in the system as illustrated in Fig. 9, it would help prevent the buckling of the strut. If the bending stiffness of the strut is assumed to be zero, all the disturbing loads would be resisted by the jury. This assumption results in conservative jury sizing and reduces the complexity of calculating the reaction forces acting on the jury.

If the value of $v_{Strut}$ is known, $F_{Disturbing}$ can be calculated with $F_{Disturbing} = 2Ptan(\gamma_{Strut})$ where $P$ is the axial load acting on the strut, and $\gamma_{Strut}$ is the angular deflection of the strut. The maximum value of $F_{Disturbing}$ can be reached when the jury has the highest axial deflection ($v_{Strut}$). This highest value can be used as one of the critical buckling loads in the sizing of the jury considering the equilibrium of $F_{Jury} = -F_{Disturbing}$. The jury should be designed to not have plastic deformation under the limit loads as per CS 25.305(a) [45]. Considering this constrain, the highest axial deflection of the jury will occur at its yield strain, $\varepsilon_Y$, and the highest value of $v_{Strut}$ can be calculated with $v_{Strut} = l_{Jury,i}\varepsilon_Y$ to compute the axial critical load acting on the jury ($F_{Jury}$).

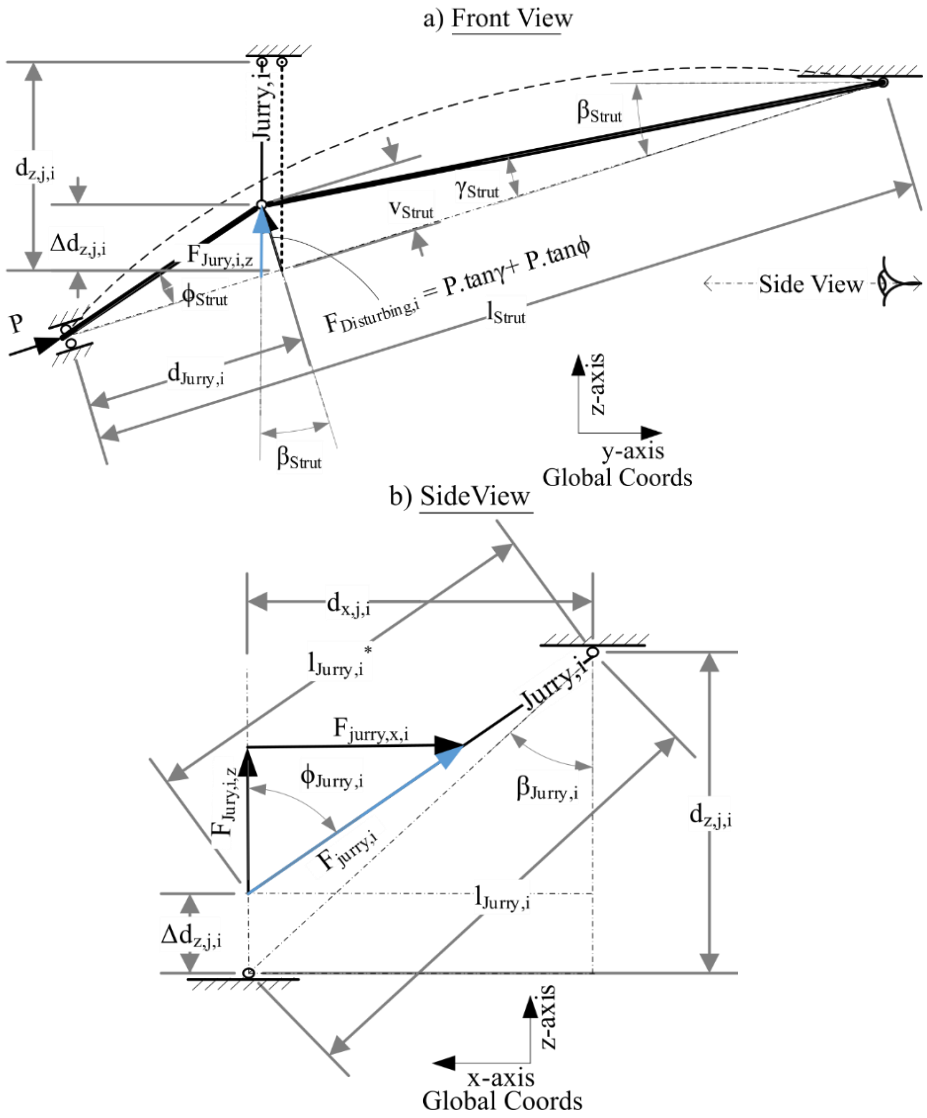


**Fig. 10 Views of the 3D TBW model to compute the axial reaction force on the jury: a) front view and b) side view.**

A similar computation procedure can be applied to the 3D SBW model to compute $F_{Jury,i}$. The application in a 3D coordinate system is not a trivial task as the components of the deflections and the reaction forces should be considered in 3D coordinates. The author modelled the 3D system as given Fig. 10 for the jury oriented perpendicular to the wing and derived the formula to compute the axial loads acting on the jury using the well-known geometric relations, and the procedure explained above. A similar model is also generated when the jury is positioned perpendicular to strut and inclined to the wing. The formulations to compute the axial reaction force acting on the jury normal to the wing, $F_{Jury,NW,i}$, and normal to the strut, $F_{Jury,NS,i}$, are given in Equations (4a) and (4b), respectively.

$$F_{Jury,NW,i} = \left( P\frac{d_{z,Jury,i} - \sqrt{\left(l_{Jurry,i} - \varepsilon_Y l_{Jurry,i}\right)^2 - {d_{x,Jury,i}}^2}}{d_{Jury,i}cos\beta_{Strut}} + P\frac{d_{z,Jury,i} - \sqrt{\left(l_{Jurry,i} - \varepsilon_Y l_{Jurry,i}\right)^2 - {d_{x,Jury,i}}^2}}{cos\beta_{Strut}\left(l_{Strut} - d_{Jury,i}\right)} \right) \frac{l_{Jurry,i} - \varepsilon_Y l_{Jurry,i}}{cos\beta_{Strut} * \sqrt{\left(l_{Jurry,i} - \varepsilon_Y l_{Jurry,i}\right)^2 - {d_{x,Jury,i}}^2}} \quad (4a)$$

$$F_{Jury,NS,i} = P\left(\frac{\frac{d_{z,Jury,i}}{cos\beta_{Strut}} - \sqrt{\left(l_{Jurry,i} - \varepsilon_Y l_{Jurry,i}\right)^2 - {d_{x,Jury,i}}^2}}{d_{Jury,i}} + P\frac{\frac{d_{z,Jury,i}}{cos\beta_{Strut}} - \sqrt{\left(l_{Jurry,i} - \varepsilon_Y l_{Jurry,i}\right)^2 - {d_{x,Jury,i}}^2}}{(l_{Strut} - d_{Jury,i})}\right)\frac{l_{Jurry,i} - \varepsilon_Y l_{Jurry,i}}{\sqrt{\left(l_{Jurry,i} - \varepsilon_Y l_{Jurry,i}\right)^2 - {d_{x,Jury,i}}^2}} \quad (4b)$$

where $d_{x,Jury,i}$, $d_{z,Jury,i}$ are the distances between the tip and the root of the jury in the x and z axes, respectively, $l_{Jurry,i}$ is the length of the jury, $d_{Jury,i}$ is the distance between the strut root and the attachment point of the jury to the strut, $\alpha_{Strut}$ is the angle between the jury and the normal of the strut surface, and $\beta_{Strut}$ is the angle between the wing and the strut reference lines.

*2. Application with Two Juries*

The simplified TBW design with two juries is illustrated in Fig. 11. It can be observed that the second jury attached at point B contributes to resisting the disturbing forces caused by the compressive load *P* and reduces the axial load carried by the first jury attached at point A. The restoring effect of the second jury (B) is neglected to reduce the complexity and have a more conservative jury sizing model while sizing the first jury (A). And the same assumption is applied in sizing the second jury. Hence, the above-given methods are also applied to the two juries' model.

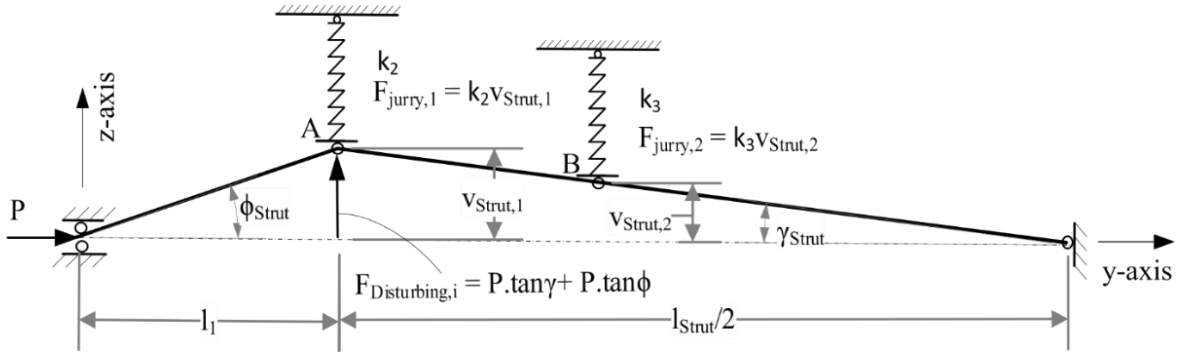


**Fig. 11 Strut design with two juries.**

Such a simplified approach is preferred considering the minimal proportion of the jury mass in wing total mass and the significantly increased complexity with more detailed analysis. It is observed that the axial loads explained in this section are generally smaller than the previously explained aerodynamic loads which drive the structural sizing of the juries. This outcome verifies the presented approaches. The validations of these methods are shown in Section V by comparing the mass of the sized juries with those of a TBW aircraft designed with higher-fidelity level methods.

**Table 4 Sizing constraint used for the truss components: strut, offset, jury-1, and jury-2.**

| Sizing Constraints | Applied for |
|---|---|
| Euler Column Buckling | Strut, Offset, Jury-1, Jury-2 |
| Strength at Yield or Ultimate Stress | Strut, Offset, Jury-1, Jury-2 |
| Bending Resistance | Offset, Jury-1, Jury-2 |
| Local Buckling of the Tube | Strut, Offset, Jury-1, Jury-2 |

## IV. Structural Sizing

The TBW structure is a frame comprising the strut, offset, juries, wing, and fuselage. The frame can be designed with and without an offset. This section explains the development of the sizing methods for TBW components by applying the sizing constraints listed in Table 4 for rectangular box model shown in Fig. 4.

### A. Load Cases

The previous section presented the load analysis of the truss components for a single flight case. These procedures must be repeated for various load cases generated through combinations of different manoeuvre directions, altitudes, fuel and payload capacities, and speed variations, as specified by CS-25 [45]. Although airworthiness requirements may evolve for novel aircraft designs, they remain a fundamental reference for load analysis and structural design.

The proposed method adopts the same load cases as the baseline method, as it represents one of the most comprehensive load sets used in quasi-analytical mass estimation studies in literature. Ref. [41] also examined the application of the baseline method to TBW (Truss-Braced Wing) configurations; accordingly, taxi and landing load cases are considered in detail, as they are expected to induce strut buckling, a dominant sizing constraint discussed in the following sections.

The baseline method [41] includes a sub-module that generates 483 load cases and corresponding flight envelopes in compliance with CS-25 regulations [45]. These cases include discretized gusts, symmetric manoeuvres, rolling (including arrest, initiation, and steady phases) and combined cases, one taxi bump case (representing inertial loads only), and one landing case (representing both aerodynamic and inertial loads).

### B. Strength at Yield or Ultimate Stresses

The primary load-carrying boxes of truss components should not exceed the yield or ultimate stress under the tensile or compression loads. This critical normal stress acting on the box due to the compressive or tensile loads can be calculated by Eq. (5) by dividing the axial load, $P$ with the cross-sectional area of the rectangular box in Fig. 4.

$$\sigma = \frac{P}{2(w_{Comp,box,j} * t_{Comp,Skin} + t_{Comp,box,j} * t_{Comp,Skin})} \tag{5}$$

If Eq. (5) is rearranged for yield stress and the $t_{Comp,Skin}$ is isolated, the skin thickness of the rectangular box (shown in Fig. 4) for strength criteria, $t_{Comp,Skin,St}$, can be computed with Eq. (6). In Eq. (6), the yield stress ($\sigma_Y$) is used for isotropic materials under limit load conditions. For quasi-isotropic composite materials subjected to ultimate loads, the ultimate stress ($\sigma_U$) is used instead of the yield stress. Ultimate loads are typically 1.5 times the limit loads as prescribed by airworthiness requirements (CS 25.303) [45].

$$t_{Comp,Skin,St,j} = \frac{P}{2\sigma_Y(w_{Comp,box,j} + t_{Comp,box,j})} \tag{6}$$

### C. Bending Resistance

Bending stresses are expected to dominate the sizing of the offset and the juries. The maximum axial stress on the rectangular box due to the bending moment, tensile or compression loads, $P$, are calculated with Eq. (7).

$$\sigma_{Max} = -\frac{M_x y_o}{I_{xx}} + \frac{M_y x_o}{I_{yy}} + \frac{P}{A_{Comp,box,j}} \tag{7}$$

where $M_x$, $M_y$ are the bending moments around the x and y axes; $I_{xx}$, $I_{yy}$ are the second moment of area around the x and y axes, and $A_{Comp,box,j}$ is the cross-sectional area of the skin of the rectangular box. If $I_{xx}$, $I_{yy}$, and $A_{Comp,box,j}$ are derived using the rectangular box model in Fig. 4, substituted in Eq. (7), and rearranged for yield stress ( $\sigma_Y$), and the term $t_{Comp,Skin,Bd}$ is isolated, the minimum thickness, $t_{Comp,Skin,Bd}$, to resist the bending moment combined with the axial loads can be computed with Eq. (8). The yield stress ($\sigma_Y$) can be changed with the ultimate stress ($\sigma_U$) under ultimate loads for quasi-isotropic composite materials.

$$t_{Comp,Skin,Bd,j} = \left| \left( + \frac{6M_x y_o}{\left(3w_{Comp,box,j} * {t_{Comp,box,j}}^2 + {t_{Comp,box,j}}^3\right)} - \frac{6M_y x_o}{\left(3t_{Comp,box,j} * {w_{Comp,box,j}}^2 + {w_{Comp,box,j}}^3\right)} + \frac{P}{2(w_{Comp,box,j} + t_{Comp,box,j})} \right) \frac{1}{\sigma_Y} \right| \tag{8}$$

### D. Euler Column Buckling

The well-known equation of the Euler column buckling for the first buckling mode is given in Eq. (9).

$$P_{Cr,1} = \frac{\pi^2 E I_{xx}}{{l^*_{Ef,Comp}}^2} \tag{9}$$

where $E$ is the material young modulus, $l^*_{Ef,Comp}$ is the effective length of the column considering the boundary conditions and the number and locations of the juries. From the inspection, it can be noticed that buckling will occur around the $x_{local}$ axis of the rectangular box given in Fig. 4. If the second moment of area of the rectangular box ($I_{xx}$) is derived for the rectangular box, substituted in Eq. (9), and $t_{Comp,Skin}$ is isolated, then the minimum panel thickness to resist the column buckling ($t_{Comp,Skin,Bk,j}$) can be computed with Eq. (10).

$$t_{Comp,Skin,Bk,j} = \frac{6P_{Cr,1}{l^*_{Ef,Comp}}^2}{\pi^2 E(3w_{Comp,box,j} * {t_{Comp,box,j}}^2 + {t_{Comp,box,j}}^3)} \tag{10}$$

where $P_{Cr,1}$ is the axial load acting on the component, $l^*_{Ef,Comp}$ is the effective length, which can be computed based on the component length ,$l^*_{Comp}$, and the boundary conditions shown in
[43]. For the strut, for instance, the length of the component, $l^*_{Comp}$, corresponds to the strut section length ($l^*_{Strut}$).

**Table 5 Colum effective length ratios for different boundary conditions [43].**

| Column Ends | $l^*_{Ef,Comp}/l^*_{Comp}$ |
|---|---|
| Both pinned | 1.0 |
| Both fixed | 0.5 |
| One fixed, the other pinned | 0.6998 |

In this study, Euler's formulation is used to assess global buckling of truss components, assuming slender column behaviour. Although slenderness ratios were not explicitly checked, the method's validity is supported by the validation study and the optimization study in Section V.E, which matched the reference SUGAR-TBW (introduced in Section V.D) results across a wide design space, including potentially low-slenderness cases. This confirms the approach remains valid for the configurations considered. Future works are recommended to explore short-column or tangent modulus-based methods for more compact or heavily loaded truss components. Additionally, more detailed buckling analyses under realistic loading conditions are recommended.

### E. Local Buckling

The rectangular load-carrying boxes of the strut, jury and offset are prone to local buckling under compressive loads. A simple, critical local buckling stress calculation process is provided in Ref. [46] with Eq. (11) for tubular struts. The component length is assumed to be at least four times longer than the structural box width or thickness.

$$\sigma_{LocalBuck} = KE_{Material}\left(\frac{t_{Comp,Skin}}{w_{Comp,Box}}\right)^2 \tag{11}$$

The critical buckling stress ($\sigma_{LocalBuck}$) can be related to the compressive load ($P_{Axial}$) with $\sigma_{LocalBuck} = P_{Axial}/A_{Comp,Box}$. If this equation, and $A_{Comp,Box}$ are substituted in Eq. (11) and the $t_{Comp,Skin}$ is isolated, the minimum skin thickness of the rectangular box to resist the local buckling stress, $t_{Comp,Skin,LB}$, can be computed with Eq. (12).

$$t_{Comp,Skin,LB} = \left(\frac{P_{Axial}w_{Comp,Box}}{2K_{Local}E_{Comp}\left(w_{Comp,box,j} + t_{Comp,box,j}\right)}\right)^{\frac{1}{3}} \tag{12}$$

$$K_{Local} = -18.702(a)^5 + 53.638(a)^4 - 61.223(a)^3 + 34.015(a)^2 - 10.41(a) + 6.245 \tag{13}$$

where $a$ is equal to $t_{Comp,box,j}/w_{Comp,box,j}$, the term, $K_{Local}$, is a coefficient and it can be computed with Eq. (13) which is generated from Fig. 2 of Ref. [46] using a 5th-order polynomial curve fitting with an $R^2$ value of 0.9997 considering that the ratio of the skin thicknesses of the short and long edges of the rectangular box (Fig. 4) is 1.

### F. Selected Thickness

In the previous sections, the formulations are derived to compute the minimum skin thicknesses of the rectangular box model under one load case considering each of the sizing criteria listed in Table 4. The thickness value under a specific load case , $t_{Comp,Skin,j,n}$, is determined by selecting the maximum among the computed skin thicknesses, such that $t_{Comp,Skin,j,n} = \max(t_{Comp,Skin,Bk,j}, t_{Comp,Skin,St,j}, t_{Comp,Skin,Bd}, t_{Comp,Skin,LB})$ where $j$ denotes the section number and $n$ denotes the load case number. This procedure should be repeated for $N_{Case}$ number of load cases explained in Section A. The final skin thickness ($t_{Comp,Skin,Selected,j}$) of the rectangular box is the maximum thickness in the list of $t_{Comp,Skin,j,n}$ as given in $t_{Comp,Skin,Selected,j} = max(\{t_{Comp,Skin,j,i,n} : n = 1, \dots, N_{Case}\})$ where $N_{Case}$ is the total number of flight cases considered.

### G. Fixed Leading and Trailing Edges Sizing

The fixed LE of the lifting surfaces must resist bird strikes in accordance with CS 25.631 [45] ensuring safe flight after the impact of a 1.81 kg bird flying at cruise speed ($V_C$) at sea level or $0.85V_C$ at an altitude of 2438 m. The procedure explained in Ref. [47] is used in this study to compute the thicknesses of the LE of truss components, including the strut, offset and jury, as given in Eq. (14).

$$t_{Comp,LE,Skin,BS,j} = 0.02V_M m^{\frac{1}{3}} f(Mat) cos^{\frac{2}{3}}\theta / [\exp(1230/(r^2 + 30r + 1000))] \quad (14)$$

where, $t_{Comp,LE,Skin,BS,j}$ is the skin thickness of the LE of the component (mm), $r$ is the leading edge nose radius (mm), $m$ is the mass of the bird (kg), $V_M$ is the impact velocity, $\theta$ is the inclination of the bird's strike direction to the normal of the surface. $f(Mat)$ represents a material factor, defined as $0.8[f_1(Mat)/f_1(L73)]$, where $f_1(Mat)$ denotes the 0.1% proof stress of the selected material, and $f_1(L73)$ refers to the 0.1% proof stress of the light alloy material, specified as L73.

Considering the simplicity of the calculation process, the same procedure is also employed to size the fixed TE thickness ($t_{Comp,TE,Skin,BS,j}$) of the truss components with more representative values of $\theta$. It ($\theta$) is taken 0 degrees for the LE and 30 degrees for the TE sizing.

## V. Mass Estimation and Validation Studies

This section explains the proposed mass estimation methods for the strut, jury, and offset and their combination with the baseline method. The proposed methods are validated with the available mass breakdown data of an aircraft with a high aspect ratio TBW from NASA's SUGAR project [48]. The mass estimation methods are also verified by comparing the optimized strut attachment location for a minimum total TBW mass to the results obtained with higher fidelity methods in Ref. [48]. The validation studies of the baseline method [41] is also briefly presented.

### A. Mass estimation of Wing Secondary Structures

As explained in Section I, this study proposes a quasi-analytical mass estimation approach that blends analytical methods for primary structural components with semi-empirical and empirical methods for secondary structures. A similar methodology was employed in the baseline method used for the prediction of cantilever wing masses [41].

The baseline method combines analytical techniques for estimating the mass of primary wing structures with existing empirical and semi-empirical methods for secondary structures. These existing methods were selected after evaluating multiple alternatives to minimize the error in mass estimations. Given the similarity between a TBW (Truss-Braced Wing) and a cantilever wing—apart from the addition of truss components—the secondary structure mass estimation methods from Ref. [41] were expected to be applicable to the TBW configuration. Furthermore, the accuracy of these secondary structure methods is validated in this study for a TBW aircraft. When more detailed data become available for future SBW or TBW designs, semi-empirical mass estimation methods should be updated.

### B. Validation of the Baseline Method

The errors of the wing group mass estimations of the baseline method and seven existing methods from the literature for thirteen metallic cantilever wings were previously presented in Ref. [41]. The aircraft's take-off gross weights range from 18,210 kg to 322,000 kg. The aircraft with aluminium alloy cantilever wing boxes were RB-66B, C-9A, C-123B, C-133B, C-135B, C-141A, DC-8, 720, 727, 737, 747, G-159 and G-1159. The baseline method performed the highest accuracy with a standard error of 1.74 and an average error of -2.22% and its computational time was noted as less than 0.1 seconds per load case utilizing an Intel i7-11800H CPU and an octa-core 2.3 GHz computer.

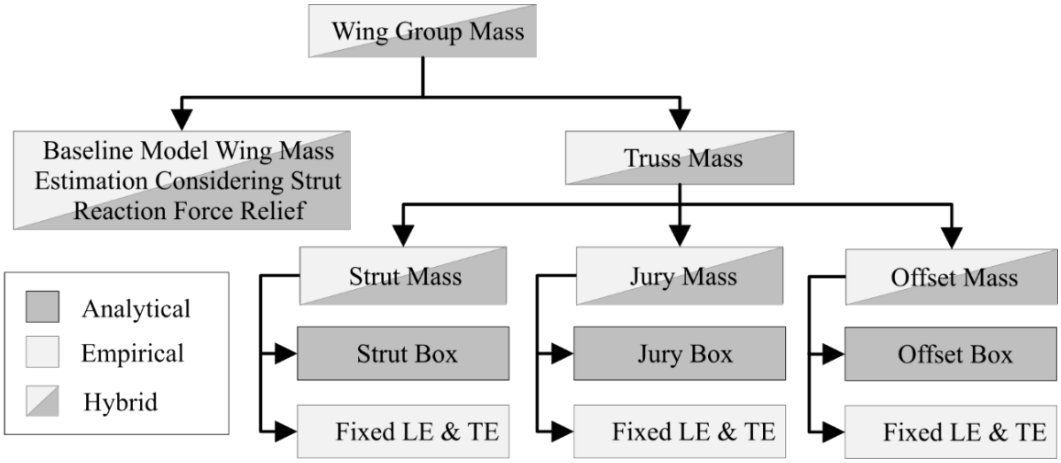


**Fig. 12 Components of the wing group mass.**

### C. Mass Estimation of Truss-Braced Wings

In the previous sections, analytical skin thickness calculation procedures are developed for the structural rectangular boxes of truss components and semi-empirical approaches are applied for the skin thicknesses of the fixed leading and trailing edges of those components as summarized in Fig. 12. The total material volume of these structural components can be computed with the selected skin thicknesses ($t_{Comp,Skin,Selected,j}$) (explained in Section IV.F) and the component lengths from the geometric models. The material masses can be computed by multiplying the computed volumes with the material densities. Similarly, the masses of LE and TE can be computed using their thickness values as explained in Section IV.G. Hence, the strut, offset, and jury masses are computed by summing the masses of their load-carrying rectangular box and their fixed LE and TE as presented in Fig. 12.

Finally, the total masses of the SBW and TBW configurations are computed by summing the truss masses and the wing mass estimated by the baseline method, while accounting for the strut reaction force relief, as illustrated in Fig. 12 and explained in Fig. 2.

### D. Validation with SUGAR Aircraft

An aircraft labelled Config 1 in Ref. [48] from the NASA's SUGAR project is selected for validation and comparison studies. The aircraft is named SUGAR-TBW in this study. The 2D top and front views of this aircraft were generated using the geometric models developed in this study and illustrated in Fig. 13. The mass breakdown[1] of SUGAR-TBW can be found in Ref. [48] . The design parameters[2] of SUGAR-TBW can be accessed in Ref. [42] which was previously presented by the author. SUGAR-TBW is a high aspect ratio TBW aircraft developed in NASA's SUGAR project employing higher fidelity level methods, including the detailed FEA, computational fluid dynamics (CFD), and nonlinear aeroelastic analysis compared to the methos proposed in this study. Hence its available data is utilized in this study, for comparison and validation studies.

Wing mass data of the SUGAR-TBW [48] is used to validate the proposed mass estimation methods for the strut and jury-1, as presented in Table 6. The quasi-isotropic material properties and the aircraft design parameter are also taken from Ref. [48]. The strut of the SUGAR-TBW is located at 58% of the wing-span length in the spanwise direction and 50% of the wing local chord in the chordwise direction. The jury is located at 50% of the strut length in the spanwise direction from the strut root and it is perpendicular to the wing.

Table 6 compares the mass estimation values computed with the proposed methods and their comparison with mass data of SUGAR-TBW in Ref. [48]. The differences between the actual and the estimated masses of the WB, strut, jury-1, and wing group are -2.25%, -15.46%, -11.29%, -6.77%, respectively. The results can be considered sufficiently accurate for conceptual and preliminary design studies compared to previously reported error values in estimating the total masses of the strut and jury with an error of +110.2% using proportional mass estimation approaches [18]. Extended validation studies with mass data from additional SBW and TBW configurations are recommended as more data becomes available.

[1] The wing mass data in Table 6, are taken from Column F of Table 2.26 in Ref. [48]. The data in column F take into account the flutter constraint of 1.15 $V_D$.

[2] Ref. [42] presents the design parameters of SUGAR-TBW in Table 6.

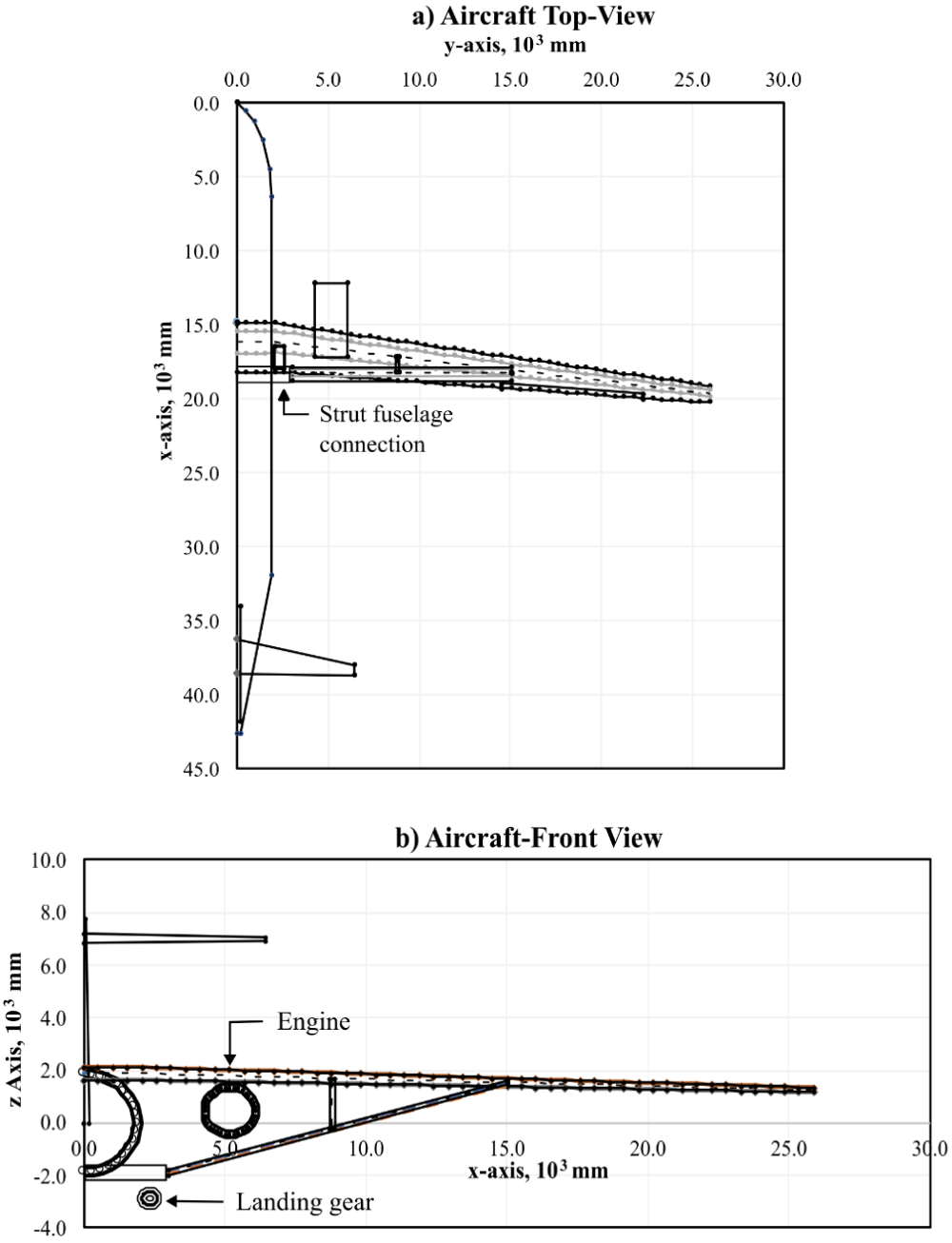


**Fig. 13 Views of the SUGAR-TBW baseline aircraft: a) top view and b) front view.**

**Table 6 Detailed validation results based on the NASA SUGAR TBW aircraft comparison.**

| | Wing Box | Strut | Jury-1 | Wing Group |
|---|---|---|---|---|
| Actual Mass [48] | 3,614.67 | 468.11 | 16.33 | 7,561.38 |
| Estimated Mass | 3,533.23 | 395.73 | 14.49 | 7,049.37 |
| Difference | -2.25% | -15.46% | -11.29% | -6.77% |

The effect of integrating the proposed method with the baseline method on the computational time is noted to be negligible. The computational time remained around 0.1 seconds per load case utilizing an Intel i7-11800H CPU and an octa-core 2.3 GHz computer. This shows the computational efficiency of the proposed methods.

These validation studies highlight the robustness and reliability of the integration of the proposed quasi-analytical mass estimation methods with the baseline method. The integrated method demonstrates significant improvements in accuracy and computational efficiency overall, making it a valuable tool for the early stages of aircraft design.

**Table 7 Optimized variables and their upper and lower bounds.**

| No | Strut Attachment (%) | Initial Values | Lower Bound | Upper Bound | Optimized Values |
|---|---|---|---|---|---|
| 1 | Spanwise location | 58 | 20 | 99 | 54 |
| 2 | Chordwise location | 50 | 15 | 65 | 25 |

### E. Verification and Comparisons with Optimum Strut Attachment Locations

The spanwise and chordwise locations of the strut-wing attachment point of the SUGAR-TBW aircraft were optimized using the global optimization method of the Differential Evolution [49] with the proposed method for a minimum wing group mass objective. The lower and upper bounds and the optimized values of the variables are given in Table 7. Chordwise bounds are chosen considering the ND chordwise positions of the front and rear spars as a fraction of the chord length.

**Table 8 Comparison of the estimated mass values of the baseline TBW and the optimized TBW with two variables.**

| | Wing Box, kg | Strut, kg | Jury, kg | Wing, kg |
|---|---|---|---|---|
| Baseline Estimated Results | 3,533.23 | 395.73 | 14.49 | 7,049.37 |
| Optimised Results | 3,534.29 | 326.55 | 11.75 | 6,978.52 |
| Difference, % | 0.03% | -17.48% | -18.89% | -1.01% |

The optimum location of the strut attachment is found at 54% span length in the spanwise direction from the root and 25% chord length from the LE in the chordwise direction as depicted in Table 7 with a minimum wing group mass of 6,978.52 kg (Table 8). This finding is close to the 58% span length position of the strut in the baseline SUGAR-TBW design [48] with the estimated wing group mass of 7,049.37 (kg). The mass reduction in the total group mass of the TBW is achieved with reduced masses of the strut and jury as presented in Table 8 due to their shortened lengths while compromising with the slightly increased mass of the WB. These outcomes verify the accuracy of the proposed method in mass estimations by comparing its optimization results to that of higher fidelity methods and illustrate the credibility of the proposed method in design exploration and optimization studies for SBW and TBW.

## VI. Results and Discussions

This section first presents the effect of the strut presence on the total mass of a high aspect ratio wing compared to the cantilever counterpart utilizing the proposed mass estimation methods. Then it investigates the application of the proposed methods for possible TBW design scenarios with hydrogen, electric, and distributed propulsion systems.

**Table 9 Comparison of wing group mass and its components for the SUGAR-CANT and SUGAR-TBW configurations.**

| Aircraft | Wing Box (kg) | Secondary Structures (kg) | Jury (kg) | Strut (kg) | Total Wing Group Mass, kg | *Mass Reduction (%)* |
|---|---|---|---|---|---|---|
| SUGAR-CANT | 5,266.1 | 3,115.9 | - | - | 8,382.0 | - |
| SUGAR-TBW | 3,523.1 | 3,115.9 | 13.7 | 392.3 | 7,044.9 | *16.0%* |

### A. The Effect of the Strut

A comparative analysis was conducted to study the impact of the strut on the reduction of WB and wing group masses. The SUGAR-TBW design parameters, explained in the previous section, are used for this study. A cantilever version of the SUGAR-TBW, called SUGAR-CANT, is generated and sized with the proposed methods to compare the effect of the strut presence on the wing group mass. The primary difference between SUGAR-CANT and SUGAR-TBW is the absence of the strut and jury in the former concept.

The results demonstrate a significant reduction of 16.0% in the wing group masses as depicted in Table 9 when utilizing the TBW configuration. The SUGAR-TBW configuration, which includes the strut and jury, shows a total wing group mass of 7,044.9 kg, while the mass of the SUGAR-CANT configuration is estimated as 8,382.0 kg. The inclusion of the strut in the TBW configuration significantly reduces the WB mass from 5,266.1 kg to 3,523.1 kg. This reduction, combined with the mass of the strut (392.3 kg) and

jury (13.7 kg), leads to an overall lighter wing group mass. The results highlight the structural advantages of the TBW design for achieving lighter wing structures.

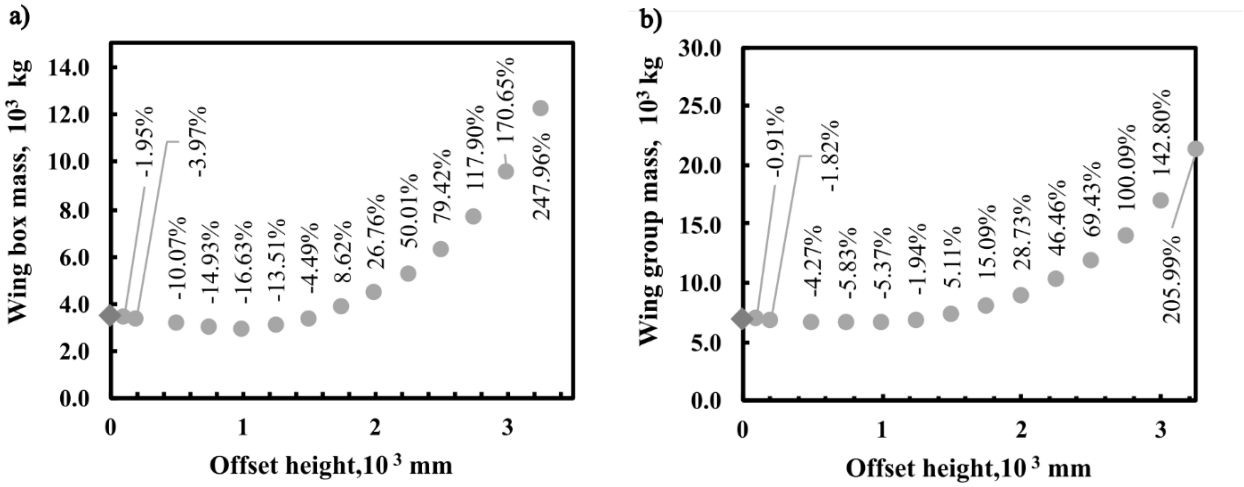


**Fig. 14 Mass variations of the a) wing group and b) wing box of the SUGAR-TBW aircraft with the change of the offset height.**

### B. The Effect of the Offset

The graphs in Fig. 14 demonstrate the variation in WB mass and wing group mass of the SUGAR-TBW configuration with change in offset height. The results reveal that adjusting the offset height can offer structural benefits in addition to its possible aerodynamic advantages in reducing the interference drag at the wing and strut attachment point as discussed in Section I.A.5. Initially, both the WB and wing group masses decrease as the offset height increases, reaching optimal values around $1\ x\ 10^3$ mm. Specifically, the WB mass shows a significant reduction of up to 16.63%, while the wing group mass achieves a reduction of approximately 5.37%. Beyond these optimal heights, both masses begin to increase, with substantial increases observed at an offset height of $3\ x\ 10^3$ mm. These findings underscore the possible dual advantage of offset height adjustments, suggesting that it should be a key consideration in future design studies to enhance both aerodynamic and structural efficiency. These preliminary findings should be investigated further with higher fidelity methods.

### C. The Effect of Distributed Propulsions

This section examines the impact of distributed propulsion on the wing group masses of SUGAR-TBW and its cantilever counterpart, SUGAR-CANT. The analysis assumes the total mass ($M_{Engine}$) and thrust ($T_{Engine}$) of the baseline propulsions of the SUGAR-TBW aircraft are evenly distributed among N engines, with each engine's mass and thrust being $(M_{Engine})/N$ and $(T_{Engine})/N$, respectively. These engines are evenly spaced along the span, positioned at intervals of $(b/2)/(N/2+1)$ on the half wing, where $b$ represents the wingspan.

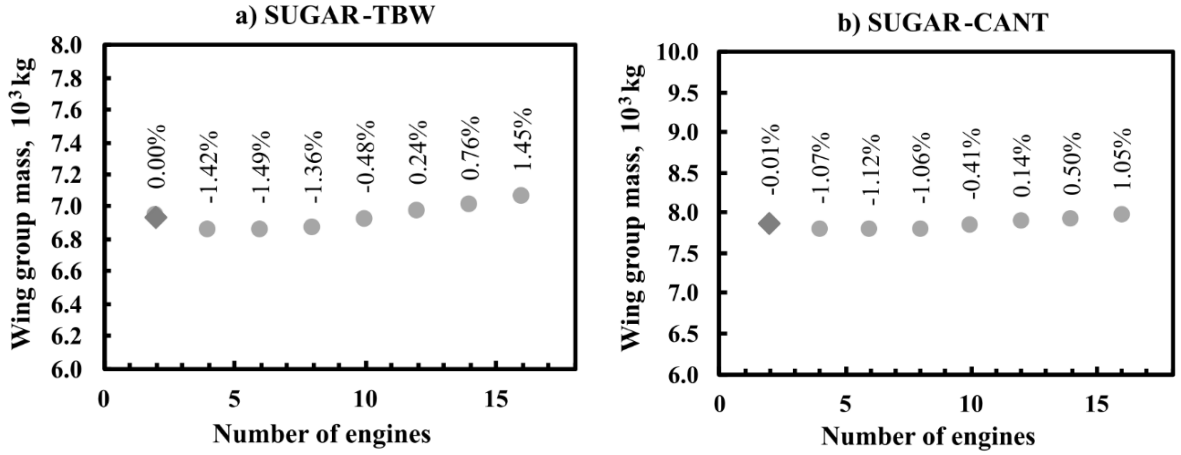


**Fig. 15 Effects of the number of engines on the wing group masses of a) SUGAR-TBW and b) SUGAR-CANT.**

Graphs in Fig. 15 illustrate the variation in wing group mass as the number of engines increases. For SUGAR-TBW, the wing group mass remains relatively stable, with changes ranging from -1.49% to +1.45%. The most significant reduction occurs with approximately five engines. Similarly, SUGAR-CANT shows minor mass fluctuations between -1.12% and +1.05%, with the greatest reduction also occurring at around five engines.

Both configurations demonstrate minimal mass variation with increasing engine counts, suggesting that distributed propulsion can be effectively integrated without significantly impacting overall wing mass. These results highlight the potential for distributed propulsion to enhance the aerodynamic performance and reduce the fuel consumption.

While the practical implementation of distributed propulsion is outside the scope of this study, the presented method offers one of the first structural sizing and mass estimation approaches to evaluate its impact. This enables early-stage design exploration of advanced propulsion concepts, with future studies expected to address operational, economic, and regulatory considerations.

Future research should also focus on high-fidelity models to verify these findings. Detailed aeroelastic analyses are recommended to better understand mass penalties associated with distributed propulsion in TBW configurations, and the proposed mass estimation methods should be refined to capture these effects more accurately.

### D. The Effect of Dry Wing Concepts

This section explores how dry wing and underwing fuel tank configurations affect the WB and wing group masses for SUGAR-TBW and -CANT aircraft, emphasizing the role of struts and underwing fuel tanks in enhancing efficiency. In this study, the term *underwing fuel tank* refers to an externally mounted fuel tank located beneath the wing. It is assumed that the total mass of hydrogen systems and fuselage-stored hydrogen fuel equals to that of the fossil fuel normally stored in the wing of the baseline SUGAR-TBW.

For the SUGAR-CANT configuration with a dry wing, the absence of wing stored fuel relief led to significant mass increases: 15.2% for the WB and 9.6% for the wing group (Table 10). However, the SUGAR-TBW configuration, which included struts, showed much lower mass increases of 2.9% for the WB and 3.0% for the wing group. The struts provided significant bending moment relief at the wing root, compensating for the missing wing stored fuel relief, and enhancing structural efficiency.

Introducing underwing fuel tanks further improved efficiency in both configurations as shown in Table 10. For SUGAR-TBW with an underwing fuel tank, the WB mass increase was 3.3%, and the wing group mass increase was 1.9%. Similarly, SUGAR-CANT with an underwing fuel tank showed reduced mass increases to 4.6% for the WB and 2.9% for the wing group.

**Table 10 Wing box and wing group masses for various configurations.**

| No | Configuration | Wing Box Mass (kg) | Difference with the Baseline (%) | Wing Group Mass (kg) | Difference with the Baseline (%) |
|---|---|---|---|---|---|
| 1 | Baseline SUGAR-TBW | 3,523 | | 7035 | |
| 2 | Dry SUGAR-TBW | 3,626 | 2.9% | 7246 | 3.0% |
| 3 | Dry SUGAR-TBW + Underwing fuel tank | 3,639 | 3.3% | 7169 | 1.9% |
| 4 | Baseline SUGAR-CANT | 5,266 | | 8382 | |
| 5 | Dry SUGAR-CANT | 6,069 | 15.2% | 9185 | 9.6% |
| 6 | Dry SUGAR-CANT + Underwing fuel tank | 5,510 | 4.6% | 8627 | 2.9% |

Overall, the integration of struts and underwing fuel tanks partially compensates for the missing fuel mass relief, significantly enhancing the structural efficiency of dry wings. Further studies using the proposed methods and more detailed mass estimations approached with higher fidelity methods are recommended for hydrogen and electric propulsion systems.

## VII. Concluding Remarks

This study presents research into the structural design and mass estimation of the strut-braced wing (SBW) and truss-braced wing (TBW) configurations, specifically integrating emerging propulsion technologies such as electric, hydrogen, and distributed propulsion systems. The findings contribute to the understanding and optimization of these advanced configurations.

The development and implementation of a quasi-analytical mass estimation method are presented. The method integrates analytical load analysis, detailed structural sizing, and mass estimation of primary and components of a TBW such as the strut, jury, and offset.

This approach not only improves computational efficiency but also enhances the accuracy of mass estimations, making it suitable for early-stage multidisciplinary design optimization (MDO) studies.

A key contribution of the study is the derivation of analytical solutions to compute the strut reaction force in a TBW configuration with distributed propulsions. This analytical solution is essential for accurate and computationally fast analytical structural sizing of TBW configurations. Additionally, methods for the load analysis of jury and offset components were developed, along with detailed procedures for their structural sizing.

The validation results demonstrate improved accuracy for conceptual or preliminary design stages with errors of -2.25% for WB mass, -15.46% for strut mass, -11.29% for jury mass, and -6.77% for wing group mass of a TBW compared to existing methods. Furthermore, the optimization study demonstrates the utility of the method for optimization applications. Comparison of the optimized strut attachment locations for the SUGAR-TBW demonstrates that the proposed method can identify optimal design parameters in close agreement with those from high-fidelity optimization studies. The minimal deviation from the previously optimized SUGAR-TBW configuration highlights the method's capability and reliability in optimization tasks.

The investigation into the effects of distributed propulsion using the proposed methods reveals minimal increases in wing group mass across varying engine counts for both SUGAR-TBW and SUGAR-CANT configurations. The minor fluctuations indicate that distributed propulsion can be effectively integrated without significant impact on the overall wing mass of the baseline aircraft, potentially enhancing aerodynamic performance and reducing fuel consumption.

The study also addresses the challenges of dry wing configurations, where fuel is stored in the fuselage rather than the wing. The introduction of struts in the wing design mitigates the adverse effects of dry wings, significantly reducing the mass penalties in WB and wing group. Incorporating underwing fuel tanks provides further alleviation in wing mass increase, demonstrating a practical solution to enhance efficiency in dry wing configurations. Notably, the study also investigates the effect of offset on the wing mass, revealing its potential in wing group mass reduction and structural advantages in addition to the aerodynamic benefits of eliminating interference drag. This dual benefit underscores the importance of considering offset in future design studies.

Future research should focus on further validation and refinements of the proposed quasi-analytical mass estimation method when more data becomes available, particularly for different configurations of TBW, propulsion technologies, and mass of the secondary structures of the strut, jury, and offset. Additionally, integrating the quasi-analytical method into MDO frameworks can reveal the full potential of the SBW and TBW configurations. Sensitivity studies can help understand the impact of different design variables on overall aircraft performance and identify critical factors that drive optimal configurations.

Overall, the proposed quasi-analytical mass estimation method provides a practical and efficient tool for early-stage aircraft design, enabling accurate and reliable optimization of advanced configurations. The proposed method paves the way for future innovations in sustainable and fuel-efficient aviation, contributing to the goal of achieving net-zero emissions in aviation.

## Acknowledgment

The first author acknowledges the support provided from the Ministry of National Education, Republic of Türkiye.

## References

[1] European Union Aviation Safety Agency (EASA), European aviation environmental report 2025., EASA, 2025. 10.2822/1537033.
[2] European Commission, Flightpath 2050: Europe's vision for aviation, European Union, Luxembourg, 2011. 10.2777/50266.
[3] D. Rajpal, R.D. Breuker, H. Timmermans, W.F. Lammen, F. Torrigiani, Including Aeroelastic Tailoring In The Conceptual Design Process Of A Composite Strut Based Wing, in: 31th Congress of the International Council of the Aeronautical Sciences, Belo Horizonte, Brazil, 2018.
[4] N. Hari, J.A. Schetz, R.K. Kapania, Numerical Prediction of Interference Drag of a Strut-Surface Intersection in Supersonic Flow, in: AIAA Scitech 2019 Forum, AIAA, San Diego, California, 2019: pp. 1–16. https://doi.org/10.2514/6.2019-0295.c1.
[5] P.J. Ansell, Hydrogen-Electric Aircraft Technologies and Integration: Enabling an environmentally sustainable aviation future, IEEE Electrification Magazine 10 (2022) 6–16. https://doi.org/10.1109/MELE.2022.3165721.
[6] M.T. Fard, J. He, H. Huang, Y. Cao, Aircraft Distributed Electric Propulsion Technologies—A Review, IEEE Trans. Transp. Electrific. 8 (2022) 4067–4090. https://doi.org/10.1109/TTE.2022.3197332.
[7] E. Moerland, T. Pfeiffer, D. Böhnke, J. Jepsen, S. Freund, C.M. Liersch, G. Pinho Chiozzotto, C. Klein, J. Scherer, Y.J. Hasan, J. Flink, On the Design of a Strut-Braced Wing Configuration in a Collaborative Design Environment, in: AIAA AVIATION Forum, AIAA, Denver, Colorado, 2017. https://doi.org/10.2514/6.2017-4397.
[8] R. Cavallaro, L. Demasi, Challenges, Ideas, and Innovations of Joined-Wing Configurations: A Concept from the Past, an Opportunity for the Future, Progress in Aerospace Sciences 87 (2016) 1–93. https://doi.org/10.1016/j.paerosci.2016.07.002.
[9] M.K. Bradley, C.K. Droney, Subsonic Ultra Green Aircraft Research: Phase I Final Report, Langley Research Center, 2011. https://ntrs.nasa.gov/search.jsp?R=20110011321.
[10] F. Linke, B. Lührs, V. Grewe, K. Kölker, R. Ghosh, I. Terekhov, M. Niklass, K. Wicke, The expected impact from the introduction of a new strut-braced wing aircraft configuration on global air traffic emissions and climate – results from the wecare project, in: 2nd ECATS Conference, Making Aviation Environmentally Sustainable, Athens Greece, 2016.
[11] F.H. Gern, A. Ko, E. Sulaeman, J.F. Gundlach, R.K. Kapania, R.T. Haftka, Multidisciplinary Design Optimization of a Transonic Commercial Transport with Strut-Braced Wing, Journal of Aircraft 38 (2001) 1006–1014. https://doi.org/10.2514/2.2887.
[12] H.D. Kim, A.T. Perry, P.J. Ansell, A review of distributed electric propulsion concepts for air vehicle technology, in: 2018 AIAA/IEEE Electric Aircraft Technologies Symposium, Cincinnati, Ohio, 2018: pp. 1–21. https://doi.org/10.2514/6.2018-4998.
[13] M.A. Gallani, L.C.S. Góes, L.A.R. Nerosky, Implementation of Distributed Electric Propulsion on a General Aviation Aircraft, in: 32nd Congress of the International Council of the Aeronautical Sciences, Shanghai, 2021.
[14] R.C. Cheung, D. Rezgui, J.E. Cooper, T. Wilson, Testing of folding wing-tip for gust load alleviation in high aspect ratio wing, in: AIAA Scitech 2019 Forum, San Diego, California, 2019: pp. 1–15. https://doi.org/10.2514/6.2019-1863.c1.

[15] N.R. Secco, J.R.R.A. Martins, RANS-based Aerodynamic Shape Optimization of a Strut-braced Wing with Overset Meshes, in: AIAA SciTech Forum, AIAA, Kissimmee, Florida, 2018. https://doi.org/10.2514/6.2018-0413.
[16] O. Dababneh, T. Kipouros, A review of aircraft wing mass estimation methods, Aerospace Science and Technology 72 (2018) 256–266. https://doi.org/10.1016/j.ast.2017.11.006.
[17] P.M. Smith, J. Deyoung, W.A. Lovell, J.E. Price, G.F. Washburn, A Study of High-Altitude Manned Research Aircraft Employing Strut-Braced Wings of High-Aspect-Ratio, NASA, Hampton, Virginia, 1981. https://ntrs.nasa.gov/citations/19810011539.
[18] G.P. Chiozzotto, Wing weight estimation in conceptual design: a method for strut-braced wings considering static aeroelastic effects, CEAS Aeronautical Journal 7 (2016) 499–519. https://doi.org/10.1007/s13272-016-0204-5.
[19] G.P. Chiozzotto, Initial weight estimate of advanced transport aircraft concepts considering aeroelastic effects, in: AIAA SciTech Forum, 2017. https://doi.org/10.2514/6.2017-0009.
[20] G.P. Chiozzotto, Conceptual Design Method for the Wing Weight Estimation of Strut-Braced Wing Aircraft, in: 5th CEAS Air & Space Conference, 2015: pp. 1–18. http://elib.dlr.de/98248/.
[21] C.E. Jobe, R.M. Kulfan, J.D. Vachal, Wing planforms for large military transports, Journal of Aircraft 16 (1979) 425–432. https://doi.org/10.2514/3.58544.
[22] A.H. Naghshineh-Pour, Structural Optimization and Design of a Strut-Braced Wing Aircraft, MSc Thesis, Virginia Polytechnic Institute and State University, 1998.
[23] F. Gern, A. Naghshineh-Pour, E. Sulaeman, R. Kapania, R. Haftka, Flexible wing model for structural wing sizing and multidisciplinary design optimization of a strut-braced wing, in: 41th AIAA/ASME/ASCE/AHS/ASC Structures, Structural Dynamics, and Materials Conference and Exhibit, AIAA, Atlanta, GA, 2000. https://doi.org/10.2514/6.2000-1327.
[24] D. Locatelli, B.K. Riggins, R.K. Kapania, J.A. Schetz, T. Poquet, A physics-based methodology for cantilever and strut-braced wing weight estimation, in: 54th AIAA Aerospace Sciences Meeting, AIAA Education Series, American Institute of Aeronautics and Astronautics, San Diego, California, USA, 2016. https://doi.org/10.2514/6.2016-0780.
[25] W. Mallik, R.K. Kapania, J.A. Schetz, Aeroelastic applications of a variable-geometry raked wingtip, Journal of Aircraft 54 (2017) 62–74. https://doi.org/10.2514/1.C033805.
[26] M. Bhatia, O. Gur, R. Kapania, W. Mason, J. Schetz, R. Haftka, Progress towards multidisciplinary design optimization of truss braced wing aircraft with flutter constraints, in: 13th AIAA/ISSMO Multidisciplinary Analysis Optimization Conference, Fort Worth, Texas, 2012. https://doi.org/10.2514/6.2010-9077.
[27] K.-S. Zhang, P.-B. Ji, A. Bakar, Z.-H. Han, Multidisciplinary evaluation of truss- braced wing for future green aircraft, in: 28th International Congress of the Aeronautical Sciences, ICAS, Brisbane, Australia, 2012. https://www.icas.org/icas_archive/ICAS2012/PAPERS/280.PDF.
[28] F. Dorbath, A Flexible wing modeling and physical mass estimation system for early aircraft design stages, PhD thesis, Technische Universität Hamburg, 2014. http://tubdok.tub.tuhh.de/handle/11420/1161.
[29] F. Hürlimann, R. Kelm, M. Dugas, K. Oltmann, G. Kress, Mass estimation of transport aircraft wingbox structures with a CAD/CAE-based multidisciplinary process, Aerospace Science and Technology 15 (2011) 323–333. https://doi.org/10.1016/j.ast.2010.08.005.
[30] A. Benaouali, S. Kachel, Multidisciplinary design optimization of aircraft wing using commercial software integration, Aerospace Science and Technology 92 (2019) 766–776. https://doi.org/10.1016/j.ast.2019.06.040.
[31] P.H. Park, Fuel Consumption of a Strutted vs Cantilever-Winged Short-Haul Transport with Aeroelastic Considerations, Journal of Aircraft 17 (1980) 856–860. https://doi.org/10.2514/3.57977.
[32] G.B. Canosa, Mass estimation of high aspect ratio wings for advanced civil airliners, MSc Thesis, Cranfield University, 2014.
[33] P.-A. Tetrault, J.A. Schetz, B. Grossman, Numerical prediction of interference drag of strut-surface intersection in transonic flow, AIAA Journal 39 (2001) 857–864. https://doi.org/10.2514/2.1389.
[34] J. Xiong, N.T. Nguyen, J. Fugate, Study of Mach 0.8 Transonic Truss-Braced Wing Aircraft Wing-Strut Interference Effects, in: AIAA SciTech Forum, AIAA, VIRTUAL EVENT, 2021. https://doi.org/10.2514/6.2021-0336.
[35] L. Liu, X. Yu, A Study on Aerodynamic Interference for Truss Braced Wing Configuration, in: International Conference on Aerospace System Science and Engineering, Springer Singapore, 2021: pp. 129–152. https://doi.org/10.1007/978-981-33-6060-0_10.
[36] J. Xiong, J. Fugate, N.T. Nguyen, Investigation of Truss-Braced Wing Aircraft Transonic Wing-Strut Interference Effects Using FUN3D, in: AIAA Aviation 2019 Forum, AIAA, Dallas, Texas, 2019. https://doi.org/10.2514/6.2019-3026.
[37] A.S.G. Ã, G. Doulgeris, R. Singh, Challenges of future aircraft propulsion: A review of distributed propulsion technology and its potential application for the all electric commercial aircraft, Progress in Aerospace Sciences 47 (2011) 369–391. https://doi.org/10.1016/j.paerosci.2010.09.001.
[38] J. Agte, O. De Weck, J. Sobieszczanski-Sobieski, P. Arendsen, A. Morris, M. Spieck, MDO: Assessment and direction for advancement-an opinion of one international group, Structural and Multidisciplinary Optimization 40 (2010) 17–33. https://doi.org/10.1007/s00158-009-0381-5.
[39] G. Flanagan, Key challenges to model-based design: distinguishing model confidence from model validation, MSc Thesis, Massachusetts Institute of Technology, 2012.
[40] A. Elham, G. La Rocca, M.J.L. Van Tooren, Development and implementation of an advanced, design-sensitive method for wing weight estimation, Aerospace Science and Technology 29 (2013) 100–113. https://doi.org/10.1016/j.ast.2013.01.012.
[41] M. Taflan, H. Smith, J. Loughlan, Structural sizing and mass estimation of transport aircraft wings with distributed, hydrogen, and electric propulsions, Aeronaut. j. (2024) 1–27. https://doi.org/10.1017/aer.2024.117.
[42] M. Taflan, H. Smith, J. Loughlan, Parametric Analysis for Structural Design and Weight Estimation of Cantilever and Strut-Braced Wing-Boxes, in: AIAA SCITECH 2023 Forum, AIAA, National Harbor, MD & Online, 2023. https://doi.org/10.2514/6.2023-1554.
[43] T.H.G. Megson, Aircraft Structures for Engineering Students, Elsevier, Oxford, United Kingdom, 2013. https://doi.org/10.1016/C2009-0-61214-9.
[44] R.C. Hibbeler, Mechanics of materials, Pearson Education, Inc, London, 2015.
[45] EASA, Certification specifications and acceptable means of compliance for large aeroplanes (CS-25), (2023).
[46] M.E. Grayley, Avoidance of buckling of some engineering elements (struts, plates and gussets), 1988.
[47] D. Howe, Aircraft Loading and Structural Layout, Professional Engineering Publishing Limited, London and Bury St Edmunds, UK, 2004. https://doi.org/10.2514/4.477041.

[48] M.K. Bradley, T.J. Allen, C.K. Droney, Subsonic ultra green aircraft research: phase II – volume I – truss braced wing design exploration, NASA Langley Research Center, Hampton, Virginia, 2015.
[49] R. Storn, Price Kenneth, Differential evolution – a simple and efficient heuristic for global optimization over continuous spaces, Journal of Global Optimization (1997) 341–359. https://doi.org/10.1023/A:1008202821328.

DSPACE

https://dspace.org/

# Sizing and mass estimation of truss-braced wings, considering emerging propulsion systems

**Taflan, Murat; Smith, Howard; Loughlan, Joseph**

**2026-01**
American Institute of Aeronautics and Astronautics (AIAA)
https://doi.org/10.2514/1.c038402
Taflan M, Smith H, Loughlan J. (2026) Sizing and mass estimation of truss-braced wings, considering emerging propulsion systems. Journal of Aircraft, Volume 63, Issue 1, January 2026, pp. 194-208

Downloaded from a DSpace repository. https://dspace.org/